Whole-animal connectome and cell-type complement of the three-segmented *Platynereis dumerilii* larva

Csaba Verasztó[1,$], Sanja Jasek[1], Martin Gühmann[2*], Réza Shahidi[1], Nobuo Ueda[2#], James David Beard[1], Sara Mendes[2], Konrad Heinz[1], Luis Alberto Bezares-Calderón[1], Elizabeth Williams[1], Gáspár Jékely[1]

[1]Living Systems Institute, University of Exeter, Stocker Road, Exeter, UK
[2]Max Planck Institute for Developmental Biology, Tübingen, Germany
[*]Current address: School of Biological Sciences, University of Bristol, Bristol, UK
[$]Current address: École Polytechnique Fédérale de Lausanne (EPFL), Lausanne, Switzerland
[#]Current address: Okinawa Institute of Science and Technology Graduate University, Okinawa, Japan
Correspondence: g.jekely@exeter.ac.uk

Abstract

Nervous systems coordinate effectors across the body during movements. We know little about the cellular-level structure of synaptic circuits for such body-wide control. Here we describe the whole-body synaptic connectome and cell-type complement of a three-segmented larva of the marine annelid *Platynereis dumerilii*. We reconstructed and annotated over 1,500 neurons and 6,500 non-neuronal cells in a whole-body serial electron microscopy dataset. The differentiated cells fall into 180 neuronal and 90 non-neuronal cell types. We analyse the modular network architecture of the entire nervous system and describe polysynaptic pathways from 428 sensory neurons to four effector systems – ciliated cells, glands, pigment cells and muscles. The complete somatic musculature and its innervation will be described in a companion paper. We also investigated intersegmental differences in cell-type complement, descending and ascending pathways, and mechanosensory and peptidergic circuits. Our work provides the basis for understanding whole-body coordination in annelids.

Introduction

Nervous systems coordinate behaviour, physiology and development through synaptic and neuroendocrine signalling. Signalling occurs specifically between groups of cells, organised into multilayered networks with precise synaptic and neuromodulatory connectivity (Bentley et al., 2016). Mapping such synaptic and chemical networks in blocks of neural tissue is the central aim of cellular-level connectomics (Deng et al., 2019; Helmstaedter, 2013; Morgan and Lichtman, 2013; Williams et al., 2017). For synaptic networks, connectomics requires volume imaging by serial electron microscopy (serial EM) (Schlegel et al., 2017).

The comprehensive analysis of whole-body coordination of actions by synaptic circuits would benefit from the cellular-level mapping of entire nervous and effector systems. Whole-animal synaptic connectomes have so far only been described for the nematode *Caenorhabditis elegans* (Cook et al., 2019; White et al., 1986) and the tadpole larva of the ascidian *Ciona intestinalis* (Ryan et al., 2016). Circuits spanning the entire central nervous system (CNS) have also been reconstructed in the larval CNS of the fruit fly *Drosophila melanogaster* (Carreira-Rosario et al., 2018; Miroschnikow et al., 2018; Ohyama et al., 2015; Schlegel et al., 2016) and in the three-day-old larva of the annelid *Platynereis dumerilii* (Bezares-Calderón et al., 2018; Randel et al., 2015;

Verasztó et al., 2017a). Recently, whole-brain connectomics has become possible in the adult fly brain (Zheng et al., 2018).

Here we report the complete synaptic connectome and cell-type complement of a three-day-old larva (nectochaete stage) of the marine annelid *Platynereis dumerilii*. This larval stage has three trunk segments, adult and larval eyes, segmental ciliary bands and a well-developed somatic musculature. The larvae show several behaviours, including visual phototaxis (Randel et al., 2014), UV avoidance (Verasztó et al., 2018), a startle response (Bezares-Calderón et al., 2018) and coordinated ciliary activity (Verasztó et al., 2017b). Three-day-old larvae do not yet have sensory palps and other sensory appendages (cirri), they do not feed and lack visceral muscles and an enteric nervous system (Brunet et al., 2016; Williams et al., 2015). Three-day-old larvae also lack associative brain centres such as mushroom bodies, which only develop several days later (Tomer et al., 2010).

In *Platynereis* larvae, it has been possible to integrate behaviour with synapse-level maps, transgenic labelling of individual neurons, activity imaging and gene knockouts (Bezares-Calderón et al., 2018; Verasztó et al., 2018, 2017a). Cellular-resolution gene expression atlases have also been developed for different larval stages. These can increasingly be integrated with single-cell transcriptomic atlases and synaptic circuit maps (Achim et al., 2015; Asadulina et al., 2012; Randel et al., 2014; Tomer et al., 2010; Williams et al., 2017). A recent study reported the registration of a gene expression atlas on a non-synaptic resolution EM volume in the six-day-old *Platynereis* larva (Vergara et al., 2020).

We previously reported synaptic connectomes for several whole-body circuits from the three-day-old larva. These include the visual, startle, ciliomotor, nuchal organ, and neurosecretory systems (Bezares-Calderón et al., 2018; Randel et al., 2015; Shahidi et al., 2015; Verasztó et al., 2018, 2017a; Williams et al., 2017). Here, we report the complete synaptic connectome and the cell-type complement of the three-day-old *Platynereis* larva. In a companion paper, we will report the desmosomal connectome and motoneuron innervation of the somatic musculature (Jasek et al.).

The analyses were based on the previously reported whole-body serial transmission EM volume. The full connectome reconstruction has now allowed us to uncover several new circuits and to consider all circuits in a whole-body context. We also found several neurons that span the entire length of the larva, highlighting the strength of a whole-body dataset. These cells and their circuits allow us to generate hypotheses on how whole-body coordination may be achieved by the larval nervous system. The connectome also allowed us to address long-standing hypotheses about the origin of the segmented annelid body-plan and explore patterns of circuit evolution.

Results

Serial EM reconstruction of a *Platynereis* larva

We traced and annotated all cells in a previously reported serial EM dataset of a three-day-old (72 hours post fertilisation (hpf) *Platynereis* larva (Randel et al., 2015). The dataset consists of 4,845 layers of 40 nm thin sections scanned by transmission electron microscopy (TEM). The sections span the entire body of the larva. We used the collaborative annotation toolkit CATMAID for tracing and reviewing skeleton and for annotations (Saalfeld et al., 2009; Schneider-Mizell et al., 2016). To mark the position of cell somas, we tagged the centre of each nucleus in the volume. We skeletonised cells containing projections or having an elongated morphology including muscle cells, glia and neurons. In neurons, we identified and marked presynaptic sites and connected the synapses to postsynaptic partners, in order to obtain the synaptic connectome (Figure 1, Figure 1 – figure supplement 1).

In the EM volume, we identified 8,852 cells with a soma. Their skeletons consisted of 5,519,861 nodes and had 27,943 presynaptic and 26,433 postsynaptic sites. We could not attach 16,260

fragments (861,448 nodes) to a skeleton with a soma. These fragments contained 4,070 presynaptic and 5,565 postsynaptic sites. Most of the fragments represent short skeletons of twigs that could not be traced across gaps or low-quality layers (Figure 1 – figure supplement 2). Overall, 6.4% of all nodes, 6.8% of presynaptic, and 4.7% of postsynaptic sites are on fragments and not assigned to a cell with a soma. The total construction time of all skeletons was over 3,600 hours with an additional 750 hours of review time.

Network analysis of whole-body synaptic connectivity

For the analysis of whole-body synaptic connectivity in the larva, we selected cells with presynaptic sites – representing differentiated neurons – and their postsynaptic partners. All fragments without a soma were removed. The final synaptic connectome contains 2,728 cells connected by 11,437 edges (25,509 synapses)(Figure 1, Figure 1 – Figure Supplement 3).
The connectome is a sparsely-connected network with a graph density of 0.0015. In comparison, the *Caenorhabditis elegans* hermaphrodite connectome has a graph density of 0.02 (Cook et al., 2019) and the *Ciona intestinalis* larval connectome 0.06 (Ryan et al., 2016)(Figures 1 and 2). We also defined a grouped cell-type connectome containing only cells that were assigned to a neuronal cell type and the partners of these cell-type groups (Figure 3 and see below).

	P. dumerilii 3-day-old larva	*P. dumerilii* 3-day-old larva cell-type graph	*C. elegans* hermaphrodite	*C. intestinalis* tadpole larva
Number of nodes	2728	222	357	213
Number of edges	11437	1158	3701	3105
Graph density	0.0015	0.02	0.02	0.06
Modularity	0.62	0.57	0.51	0.61
Avg. clustering coefficient	0.1	0.16	0.22	0.32
Avg. path length	5	2.9	2.9	2.7
Avg. degree	4.1	8.6	10.3	13.9

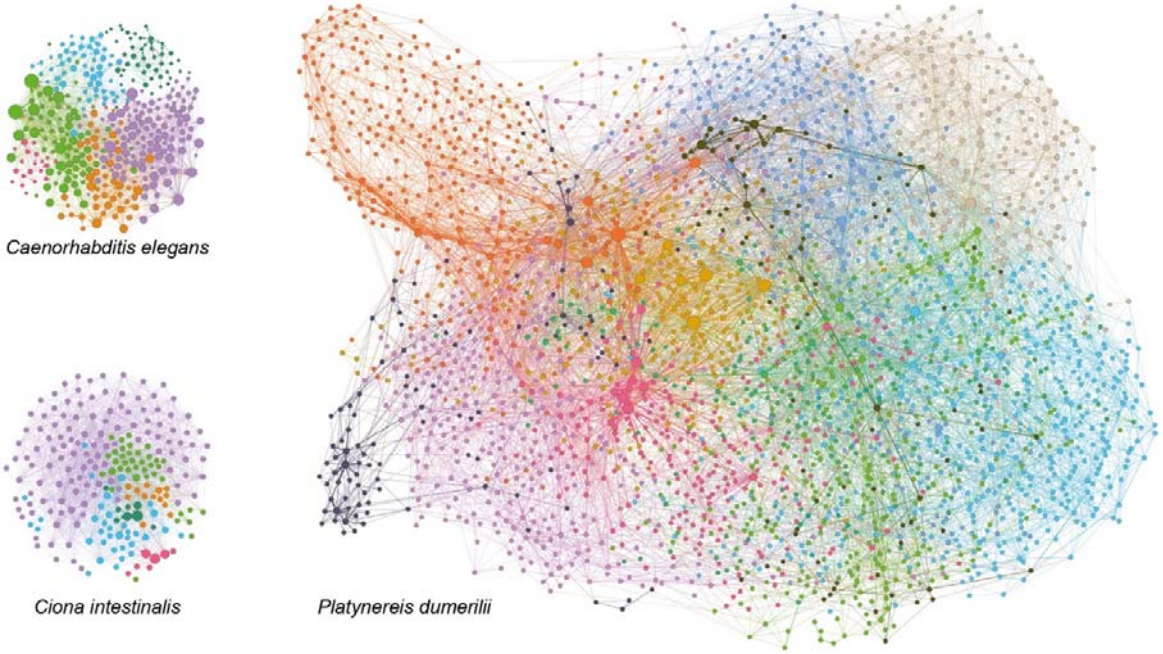

Figure 1. The *Platynereis dumerilii* larval connectome in comparison to the *C. intestinalis* and *C. elegans* connectomes.
Graphs of the *C. elegans* hermaphrodite, *C. intestinalis* tadpole larva and *P. dumerilii* three-day-old larva chemical synapse connectomes. Nodes represent individual cells, edges represent synaptic connectivity. Arrowheads were omitted. Nodes are coloured by modules. Node sizes are proportional to weighted degree.

The table shows network parameters for the connectome graphs. Figure 1 – source data 1 (adjacency matrix).

Next we used community detection to delineate more strongly connected subgraphs within the connectome. This analysis combined with force-field-based clustering revealed several modules that may represent functional units (Figures 1 and 2). We named the modules based on their primary effector organs or other dominant anatomical characters. The modules recovered include the anterior neurosecretory centre with head ciliomotor neurons, the trunk ciliomotor system, the visual circuit, a module innervating head pigment cells, a left and right module for the innervation of segmental exocrine glands, a module of projection interneurons and four muscle-motor modules. It should be noted that community analysis can produce different numbers of modules by merging or further subdivisions, depending on the parameters used.

To identify nodes of potential functional importance we analysed node centrality in the connectome graph. We ranked nodes based on degree (number of pre- and postsynaptic partners), page rank (a measure of the number and importance of incoming links) and other measures (Figure 1 – figure supplement 2, Supplementary Table 1). We also ranked the edges connecting nodes in the graph (Supplementary Table 1). Nodes with the highest degree included ciliomotor neurons (e.g. Loop, Ser-tr1)(Bezares-Calderón et al., 2018; Verasztó et al., 2017a), the sensory-motoneuron pygPBunp (Verasztó et al., 2017a), and the motoneurons of exocrine glands (MNspinning, see below). Some of the strongest edges (highest number of synapses) were between the pigment-cell motoneuron cioMNcover and prototroch pigment cells, MNspinning and exocrine glands, and the MC cell and ciliated cells (Supplementary Table 1).

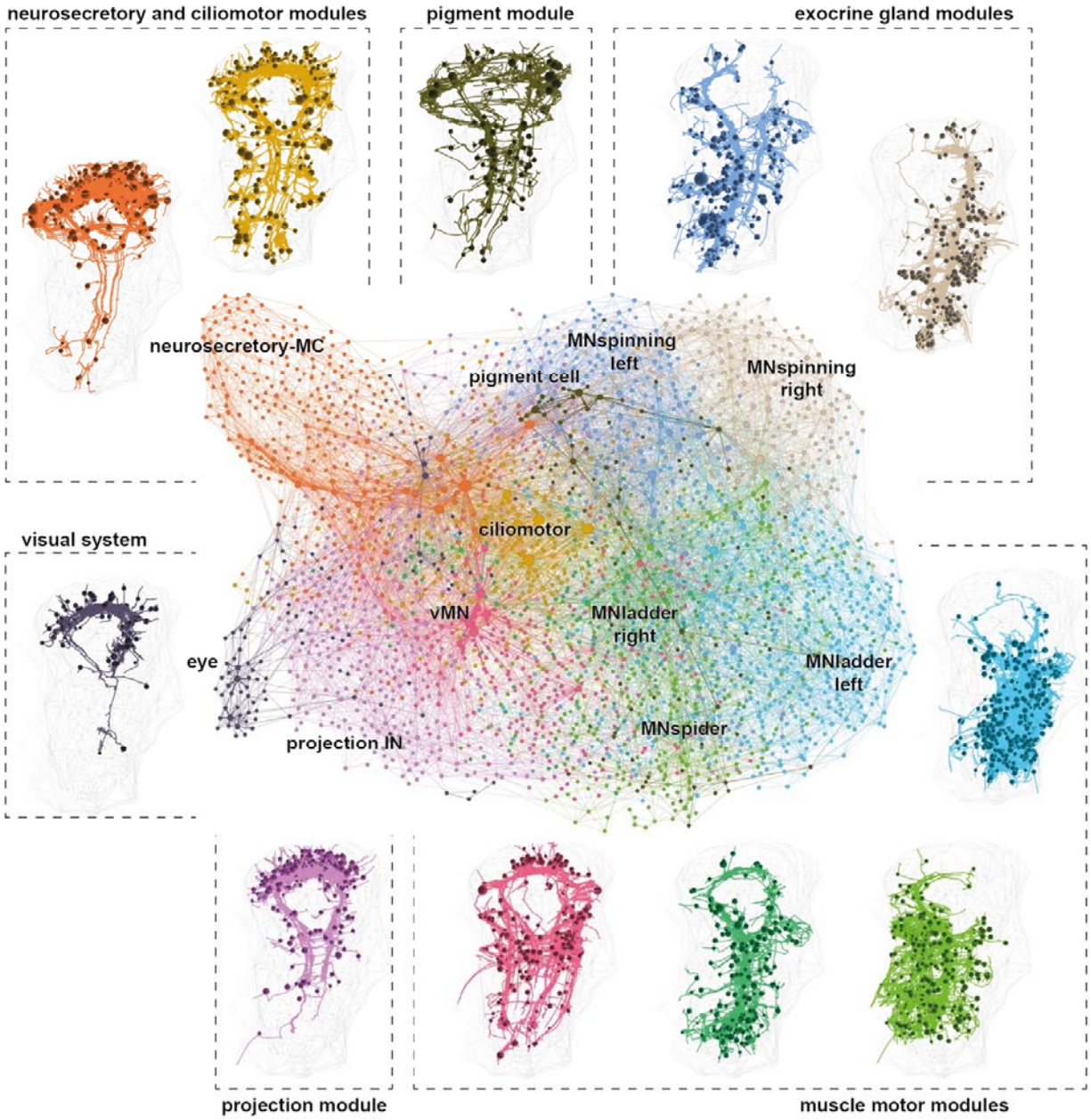

Figure 2. Modularity of the *Platynereis* three-day-old larval connectome
Graph representation of the connectome coloured by modules. Nodes represent single cells, edges represent synaptic connectivity. Arrowheads are not shown for clarity. The reconstructed cells for each module are shown. Spheres represent soma positions (centred on the nuclei).

Classification of cell types

To classify the reconstructed cells into neuronal and other cell types, we used various approaches. For a morphological classification of neurons based on the similarity of their skeleton arbots, we used Sholl analysis (Sholl, 1953) and NBLAST as implemented in CATMAID (Schneider-Mizell et al., 2016) and the `natverse` (Bates et al., 2020; Costa et al., 2016), respectively. Hierarchical clustering of distance matrices obtained from NBLAST and Sholl analysis often delineated neurons with similar arbors that we consider cell types (shown for the motoneurons in Figure 3 – figure supplement 1). These analyses however, do not use ultrastructural details (e.g. presence of sensory cilia), which we consider important for classifying cell-types. Likewise, clustering based on connectivity alone did not give sufficient resolution (data not shown).

We therefore manually classified neurons into cell types and derived a grouped cell-type graph (Figure 3). Our classification considers both morphology and connectivity. We used a combination of five criteria: i) the position of neuron somata, ii) the morphology of axon projections (e.g. branching pattern, decussation, ascending or descending), iii) the ultrastructure of sensory specialisations (e.g. number and type of cilia, microvilli – for sensory neurons only), iv) neuropeptide content as determined by the siGOLD immunolabelling method (Shahidi et al., 2015), and v) synaptic connectivity. We also required left-right symmetry for a group of similar neurons to classify as a cell type except for a few clearly asymmetric neurons (e.g. SN_YF5cil, pygPBunp). Based on these criteria, we classified 892 neurons into 180 cell types (Table 1, Video 1, Figure 3, Figure 3 – figure supplements 2 and 3).

We also categorised the remaining 7,960 cells in the larval body. 2,905 of these were classified into 90 non-neuronal cell types (Table 2). These included epithelial cells (974 cells) various pigment cells (7 types), muscle cells (852 cells of 53 types, described in the companion paper, Jasek et al.), locomotor ciliated cells (80 cells of 6 types), glial cells (3 types), gland cells (6 types), various support or sheet cells, nephridia, putative migratory cells, and parapodial cells producing or ensheathing chitin bristles (chaetae and aciculae) (Table 2, Video 2). In addition, we defined 18 broader neuronal cell groups, containing neurons of similar morphology (e.g. head decussating neurons) but in either differentiated or immature state (e.g. immature palp sensory neurons). The annotations are hierarchical, and cell groups can contain one or more differentiated cell types (Table 3).

The remaining 5,230 cells are either dividing cells (62 cells), undifferentiated cells that putatively belong to the neuronal lineage (1,692 cells) and various weakly connected or developing neurons with projections (3,476). These cells were not classified into cell types. The developing antennae contain 126 cells of which the majority (88) have few synapses and/or immature sensory dendrites. In the developing palps, we found 67 immature sensory neurons. The developing mouth (619 cells) is lined with 52 immature stomodeal sensory neurons. A further 146 immature sensory neurons and 52 non-sensory neurons occur in the dorsal head and the ventral nerve cord (VNC) (Figure 3 – figure supplement 4).

All cells were annotated in CATMAID with information representing the above categories. We also annotated all cells based on their soma position in the body (e.g. left or right side, segment 0-3, germ layer etc.; see Methods). These annotations were used to query the data and visualise subsets of cells in CATMAID or the `natverse`.

The cell-type classification allowed us to analyse a grouped synaptic connectivity graph where cells of the same type were collapsed into one node (Figure 3). This cell-type connectome included 81 sensory, 61 interneurons, 35 motoneuron types, 5 ciliated cell types, 33 muscle types, 3 glands, and 2 pigmented cell types.

By community analysis, we detected modules similar to the analysis of the full connectome graph, including ciliomotor, gland-motor, pigment-motor and muscle-motor modules (Figure 3). This cell-type graph has network parameters very similar to the *C. elegans* and *C. intestinalis* connectome graphs (Figure 1), suggesting a similar overall circuit organisation at the level of cell types, but with an order of magnitude more cells in *Platynereis*.

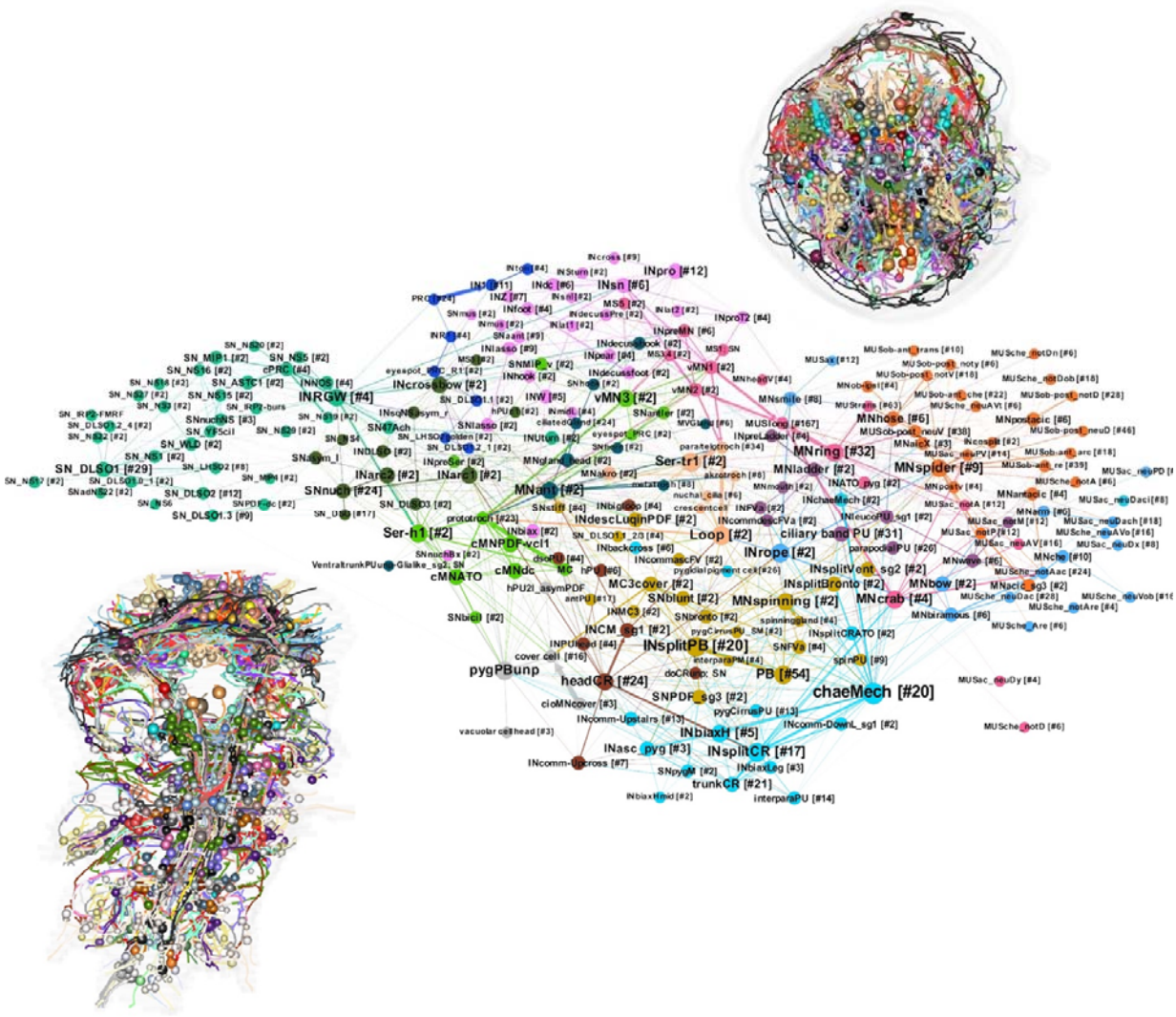

Figure 3. The grouped connectome of cell types

Grouped connectivity graph of cell types. Nodes represent groups of neurons, with the number of cells in square brackets. Edges represent synaptic connectivity. The width of arrows is proportional to the square root of the total number of synapses. Reconstructions of all cell types, individually coloured are shown in ventral (lower left) and anterior (upper right) view.

Figure 3 – source data 1. Gephi network file of the grouped cell-type connectome.

Neurotransmitter and neuropeptide identities

Through a combination of *in situ* hybridisations, transgenic labelling and serial multiplex immunogold (siGOLD) labelling done previously (Bezares-Calderón et al., 2018; Conzelmann et al., 2013; Jékely et al., 2008; Randel et al., 2014; Shahidi et al., 2015; Verasztó et al., 2017a; Vergara et al., 2017), we assigned neurotransmitters or neuromodulators to several identified neurons. These transmitters and modulators could now be mapped to the whole connectome (Figure 4). We annotated 18 cholinergic, 4 serotonergic, 1 dopaminergic, 1 adrenergic, 69 glutamatergic neurons and 123 neurons expressing one of 13 different neuropeptides (pigment dispersing factor – 31, allatotropin/orexin – 23, leucokinin – 4, proenkephalin – 2, FVamide – 15, FMRFamide – 11, other RF/RYamide – 11, myoinhibitory peptide – 6, achatin – 1, RGWamide – 6, MLD/pedal peptide – 4, IRP2 – 2, WLD – 2, FVRIamide – 5 neurons). Neuropeptides occur in sensory, motor and interneurons.

We highlight cellular and sensory-effector circuit examples for PDF, leucokinin and allatotropin/orexin neuropeptides (Figure 4F). For example, two leucokinin-expressing interneurons (INleucoPU) in the first trunk segment are postsynaptic to mechanosensory PU cells and INsplitPB neurons and synapse on MNladder, MNmouth, and MNwave motoneurons (Figure 4G). We also defined a larger network containing several peptidergic neurons. (Figure 4H)
The specific neuropeptide-expressing cells and their mini-circuits pinpoint potential sites of peptidergic modulation within the connectome.

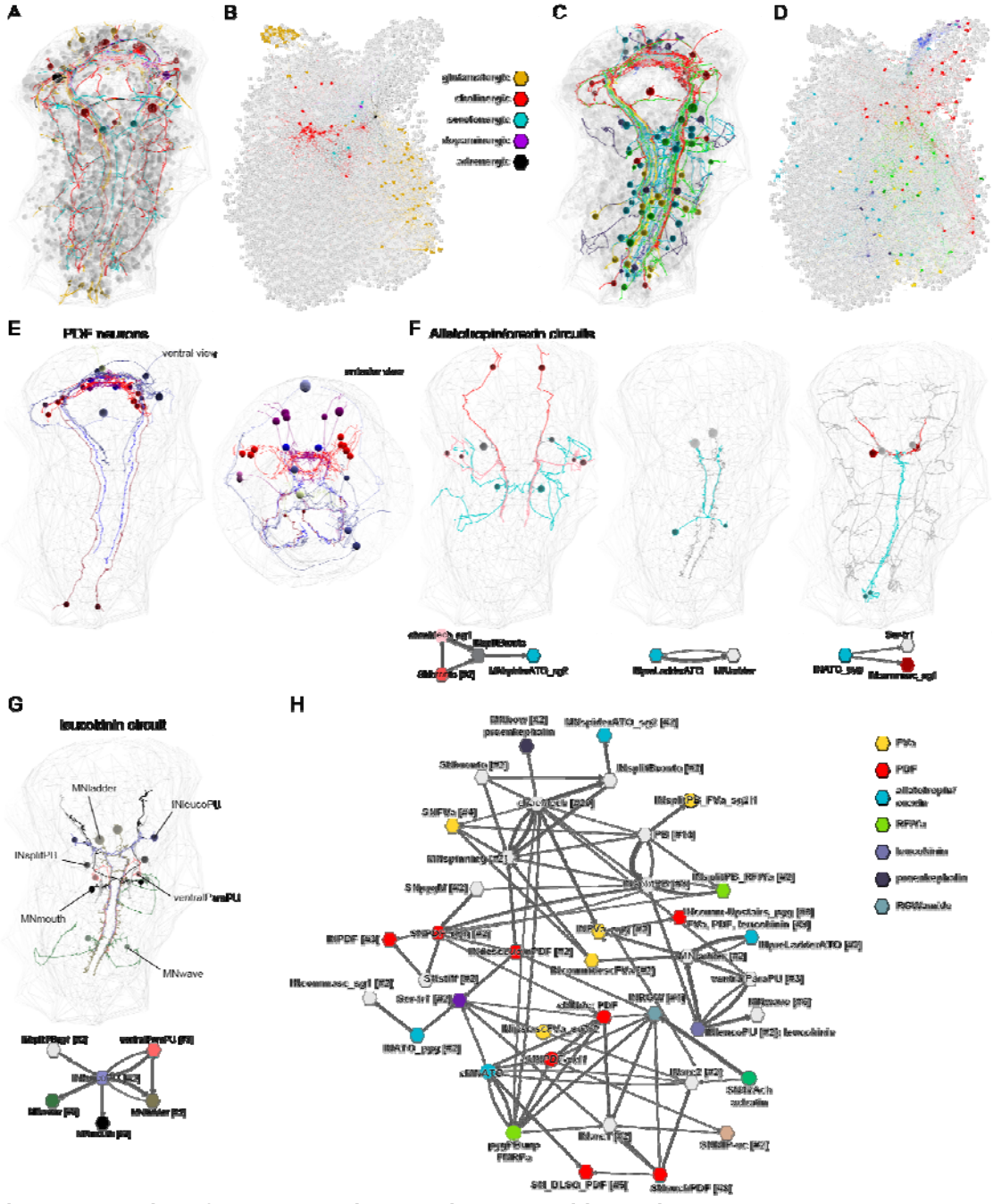

Figure 4. Mapping of neurotransmitters and neuropeptides to the connectome.
(A) Reconstructed neurons (in colour) with a known neurotransmitter profile. (B) Neurons with a known neurotransmitter profile mapped to the connectome graph. (C) Reconstructed neurons (in colour) with a known neuropeptide profile. (D) Neurons with a known neuropeptide profile mapped to the connectome graph. (E) Neurons expressing pigment dispersing factor (PDF), ventral and anterior views. (F) Local circuits of cells expressing the allatotropin/orexin neuropeptide. (G) Local circuit of two INleucoPU neurons expressing the

leucokinin neuropeptide. (H) Grouped graph of neuropeptide-expressing neurons and their pre- and postsynaptic partners. All neurons with known neuropeptide expression are shown in colour.

Multisensory convergence and interneuron-level integration

The neuronal cell types included 45 sensory neuron types with postsynaptic partners. These collectively connect to 52 primary interneuron types, defined as interneurons directly postsynaptic to sensory neurons (Figure 5). Some sensory neurons directly connect to muscle-motor, ciliomotor or pigment-motor neurons (e.g. eyespotPRC_R3, MS cells, SNhook, SNblunt) (Figure 5E, F) or to ciliated, pigmented or muscle effector cells (e.g. eyespotPRC_R3, pygPBunp, hPU2l_asymPDF, pygCirrusPU_SM)(Figure 3 – figure supplement 2). These represent more direct sensory-motor pathways.

The distribution of the number of partners is skewed with many sensory neurons only synapsing on one interneuron type and many interneurons only receiving input from one sensory neuron type (Figure 5A and B). At the other end of the distribution, the head CR and chaeMech sensory neurons have >10 interneuron partners, suggesting that they can recruit a more extended downstream circuit (Figure 5A).

Some interneurons and motoneurons are directly postsynaptic to several distinct sensory neuron types (up to 10)(Figure 5B-F). Such convergence suggests that these neurons can integrate multisensory inputs. Among the interneurons, INarc1, INasc_pyg, INbiaxH and INsplitPUh have >6 presynaptic sensory neuron partners (Figure 5B-D). The ventral head motoneurons (vMN) receive direct input from four sensory neuron types (MS mechanosensory, eyespotPRC_R3, SNantlerPDF, and SNMIP-vc sensory-neurosecretory neurons (Conzelmann et al., 2013))(Figure 5B, D). The MNant ciliomotor neurons are postsynaptic to three sensory neuron types in the ventral head (SNantlerPDF, SNhook, and SNhorn neurons).

The interneurons with the highest number of interneuron partners were a group of INW cells (Figure 5C). These neurons belong to the head ‘projection neurons’ module and connect to many pre- and postsynaptic interneuron types (to some only with few synapses). The INW neurons have decussating axons that delineate a V-shaped brain neuropil (not shown). This region may represent a developing integrative brain centre.

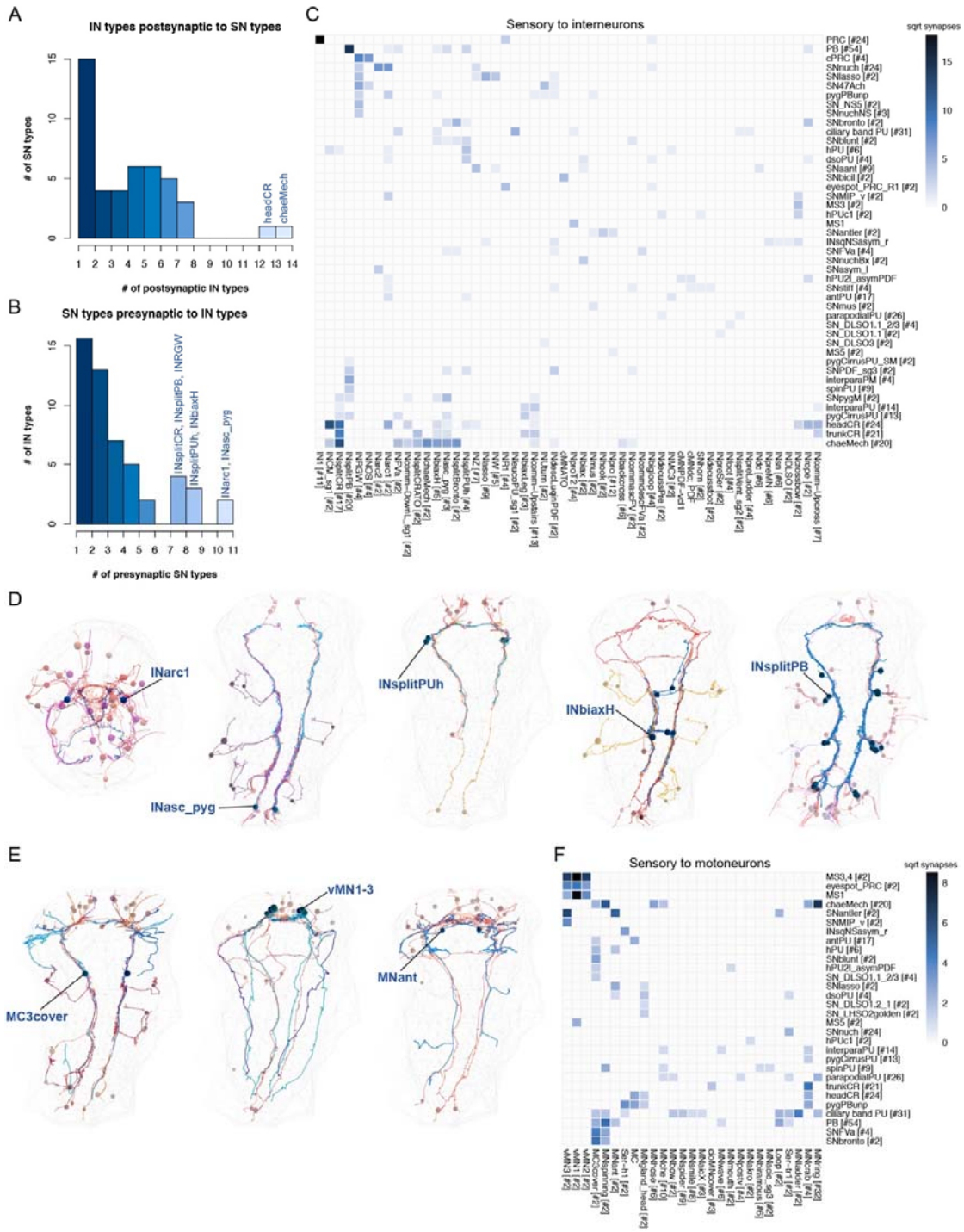

Figure 5. Connectivity of sensory neurons to primary interneurons and motoneurons.
(A) Histogram of the number of interneurons postsynaptic to each sensory neuron type (only those with postsynaptic partners). (B) Histogram of the number of sensory neurons presynaptic to each primary interneuron type (only those with presynaptic SN partners). (C) Grouped connectivity matrix of sensory neurons and their direct postsynaptic interneuron partners. Cells are grouped by type, the number of cells in each group is indicated in square brackets. (D) EM reconstructions showing five different interneuron types with their diverse presynaptic sensory cells. (E) EM reconstructions showing three different motoneuron types with their diverse presynaptic sensory cells. (F) Grouped connectivity matrix of sensory neurons and their direct postsynaptic motoneuron partners. Cells are grouped by type, the number of cells in each group is indicated in square brackets.

Descending and ascending pathways connecting the brain and the VNC

Next we analysed synaptic connectivity between the brain and the ventral nerve cord. We identified all brain neurons with descending projections into the ventral nerve cord (VNC) and all trunk neurons with ascending projections into the brain. The brain has 146 such neurons, including ipsilaterally descending sensory and interneurons and decussating inter- and motoneurons. In the trunk, we found 76 ascending neurons with axons reaching the brain neuropil. The ascending and descending neurons are highly interconnected between each other and with other head and trunk neurons (Figure 6).

Some neurons connecting the trunk and the head have a global reach, with projections spanning all trunk segments and the brain (Figure 7 C-E). We identified 40 such neurons (annotation: “global_reach”), 20 of which are part of the mechanosensory girdle (see below). In the trunk, these cells only occur in the first segment and the pygidium. The pygidial neurons (e.g. cioMNcover, SNPDF_pyg, INasc_pyg, pygPBunp) span the entire VNC and terminate in the head and synapse on head neurons or on the prototroch ciliary band and its cover cells. Similarly, some head neurons have descending projections that span all trunk segments (e.g. vMN, Ser-h1, INrope, MNgland_head). The first segment contains many unique cell types with global reach (e.g. Ser-tr1, MC3cover, Loop, INsplitPBant).

A small group of neurons with global reach are involved in body-wide ciliary coordination (Loop, Ser-tr1, Ser-h1)(Verasztó et al., 2017a) or coordinated intersegmental movements (INrope, vMN)(Bezares-Calderón et al., 2018; Randel et al., 2014). The function of the other descending and ascending cell types is not known and may relate to intersegmental motor coordination. Similar descending neurons coordinate trunk movements in *Drosophila* and leech. For example, the MDN descending neurons in the fly activate backward locomotion and suppress forward locomotion (Carreira-Rosario et al., 2018). The leech R3b-1 descending neurons are command neurons involved in intersegmental coordination (Puhl et al., 2012).

The whole-body analysis of the entire connectome allowed us to identify all ascending and descending neurons and their connections in the three-day-old larva.

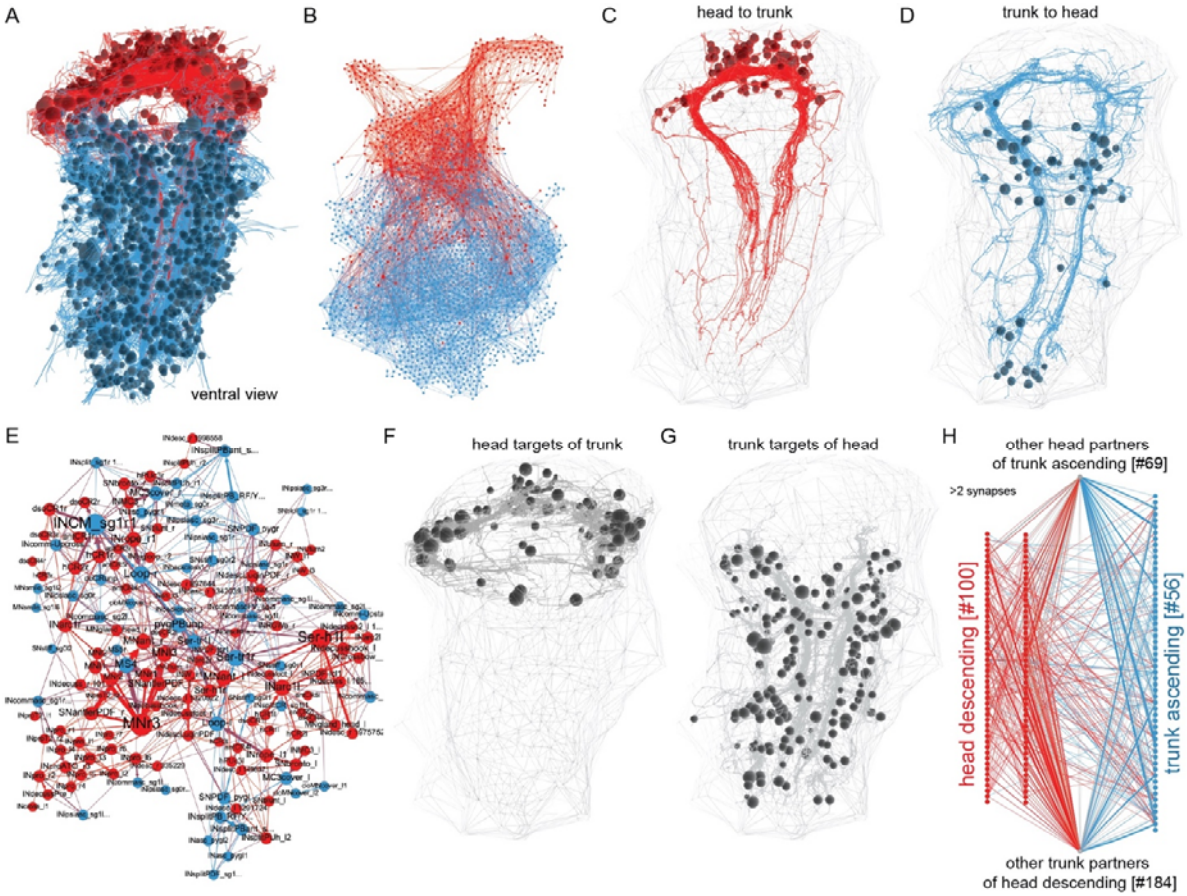

Figure 6. Interconnectedness of head and trunk circuits.
(A) Reconstructed head (red) and trunk (blue) neurons, which are part of the connectome. (B) Graph representation of head (red) and trunk (blue) neuron connectivity. (C) Skeletons of all head neurons with descending projections into the ventral nerve cord. (D) Skeletons of all trunk neurons with ascending projections into the head. (E) Interconnectivity of head descending and trunk ascending neurons. The force-field-based layout shows how head and trunk neurons intermingle (F) All head neurons (other than in C) with synaptic contacts to trunk ascending neurons (shown in D). (G) All trunk neurons (other than in D) with synaptic contacts to head descending neurons (shown in C). (H) Network representation of synaptic connectivity of the neuron groups shown in C,D,F,G. Edges represent synaptic connections and are coloured as their source node in (H) or with a colour mixing the source and target colour in B and E (edges connecting head and trunk neurons are purple).

Segment-specific and segmentally iterated cell types

The annotated whole-body connectome allowed us to compare the neuronal complement of the various segments of the *Platynereis* larval body. The three-day-old larva has three main trunk segments with chaeta-bearing parapodia (chaetigerous segments) and a more anterior cryptic segment (CATMAID annotation: segment_0) (Steinmetz et al., 2011). In addition, the pygidium forms the posterior-most part of the body (Starunov et al., 2015)(Figure 7A, E). The ciliary bands mark the posterior segment boundaries and *engrailed* expression the anterior boundary. Larval segments differ in the expression of Hox genes (Steinmetz et al., 2011). During the process of cephalic metamorphosis, the first segment loses its chaetae and fuses into the head (Fischer et al., 2010).
We identified many segment-specific and pygidium-specific neuron types and neuron types present in different subsets of segments (Figure 7 – figure supplement 1). There are 10 neuronal cell types specific to the first segment, eight to the second segment, two to the third segment and seven to the

pygidium. Neurons with global reach are only present in the first segment, the pygidium and the head (Figure 7C-E, Figure 7 – figure supplement 1).
These distinct neuron complements suggest a functional specialisation of the different trunk segments and are in agreement with segmental differences in the expression of developmental transcription factors (Vergara et al., 2017).
There are also several neuron types that are present in all chaetigerous segments (Figure 7 – figure supplement 1) including the chaeMech sensory neurons, the INsplitPB and INbackcross interneurons and the MNche and MNhose motoneurons. In addition, three sensory neuron types and two muscle types occur in the head, in all four trunk segments and the pygidium (Figure 7F-J).

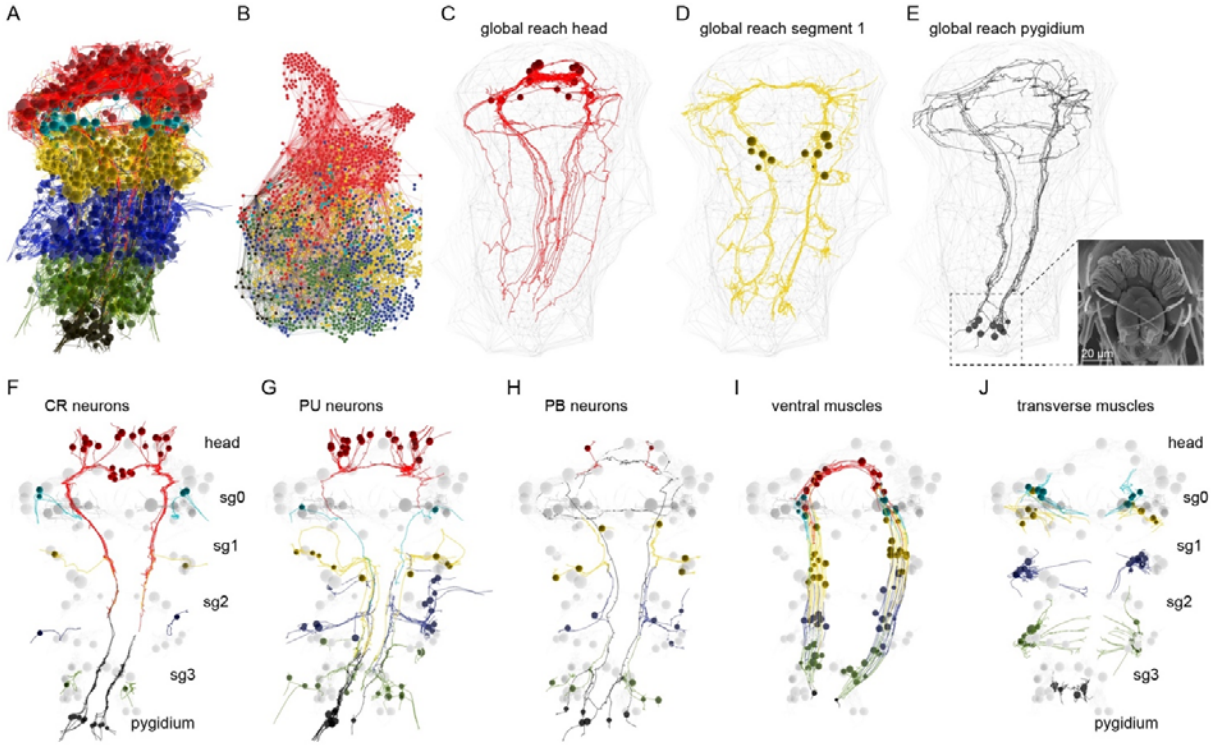

Figure 7. Segment-specific and segmentally iterated cell types.
(A) Reconstructed cells of the connectome coloured by segment. (B) Connectome graph coloured by segment (colours same as in panel A) (C) Head-specific neurons with a global reach (D) Neurons in the first segment with a global reach. Inset: SEM image of the pygidium. (E) Neurons in the pygidium with a global reach. (F) Segmentally iterated collar receptor (CR) mechanosensory neurons. (G) Segmentally iterated uniciliated penetrating mechanosensory neurons (H) Segmentally iterated biciliated penetrating mechanosensory neurons. (I) Segmentally iterated ventral longitudinal muscles (MUSlong_V). (J) Segmentally iterated transverse muscles (MUStrans).

Exocrine glands and their innervation

There are two types of non-locomotor effector systems in the *Platynereis* larva, exocrine glands and pigment cells.
Two large modules are centred around a pair of exocrine-gland motoneurons (MNspinning). These have the largest number of incoming and outgoing synapses in their respective modules (Figure 2). The two MNspinning cells synapse on two pairs of large endocrine gland cells (spinGland or spinning gland) found in the parapodia of the second and third segments.

The four spinGland cells have a large microvillar secretory pore at the tip of the ventral parapodia (neuropodia). The MNspinning motoneurons are postsynaptic to various sensory pathways, including the chateal receptors (chaeMech), two head SNbronto sensory neurons and their postsynaptic interneuron partners (INbronto). Inputs from the chaeMech receptors suggest that mechanical stimuli to the chaetae may regulate secretion from the spinGlands.

We identified five further gland-cell types in the *Platynereis* larva. These differ in their position, size, ultrastructure and innervation (Figure 8A, Figure 8 – figure supplement 1). A similar diversity of glands occurs in the epidermis of other annelids (Hausen, 2005).

In the ventral head, there are five large headGland cells. These cells are filled with large (diamer=1.4 µm, stdev=0.28 N=36) secretory vesicles and have no presynaptic partners.

In the first segment, there is a ventral girdle of gland cells containing two gland types, the ciliatedGland (24 cells) and the MVGland cells (6 cells). CiliatedGland cells have a microvillar collar and a stiff cilium penetrating the cuticle, suggesting that these are sensory-exocrine cells. MVGland cells have a broader microvillar secretory pore and no cilium. These gland cells are postsynaptic to two decussating head gland motoneurons (MNgland)(Figure 8B). The MNgland cells receive input from the rhythmically active serotonergic system (Verasztó et al., 2017a) suggesting a link between ciliary swimming and glandular secretion.

Close to the site of secretion of the large spinGlands, there is a secretory pore for the smaller, spinMicroGland cells (16 cells). SpinMicroGland cells have microvilli and secrete through a narrow tunnel in the cuticle. These spinMicroGlands receive no synapses in the three-day-old larva.

In the second segment, there are two additional interparapodial glands (interparaGland) with a small microvillar secretory pore opening in the cuticle between the neuro- and notopodia. These cells have long projections, but we could not identify synaptic inputs to them.

The various glands can also be distinguished by their glycosylated secretory content, as revealed by stainings with fluorescently labelled lectins (Figure 8 – figure supplement 1). The spinGland cells can be stained with wheat germ agglutinin (WGA) and *Lotus*, *Ulex* and *Pisum* lectins. The secretory content of headGlands can be labelled with *Griffonia*, peanut and *Pisum* lectins (Figure 8 – figure supplement 1). The girdle of ciliatedGland and MVGlandcells stains with *Griffonia* lectin (Figure 8 – figure supplement 1).

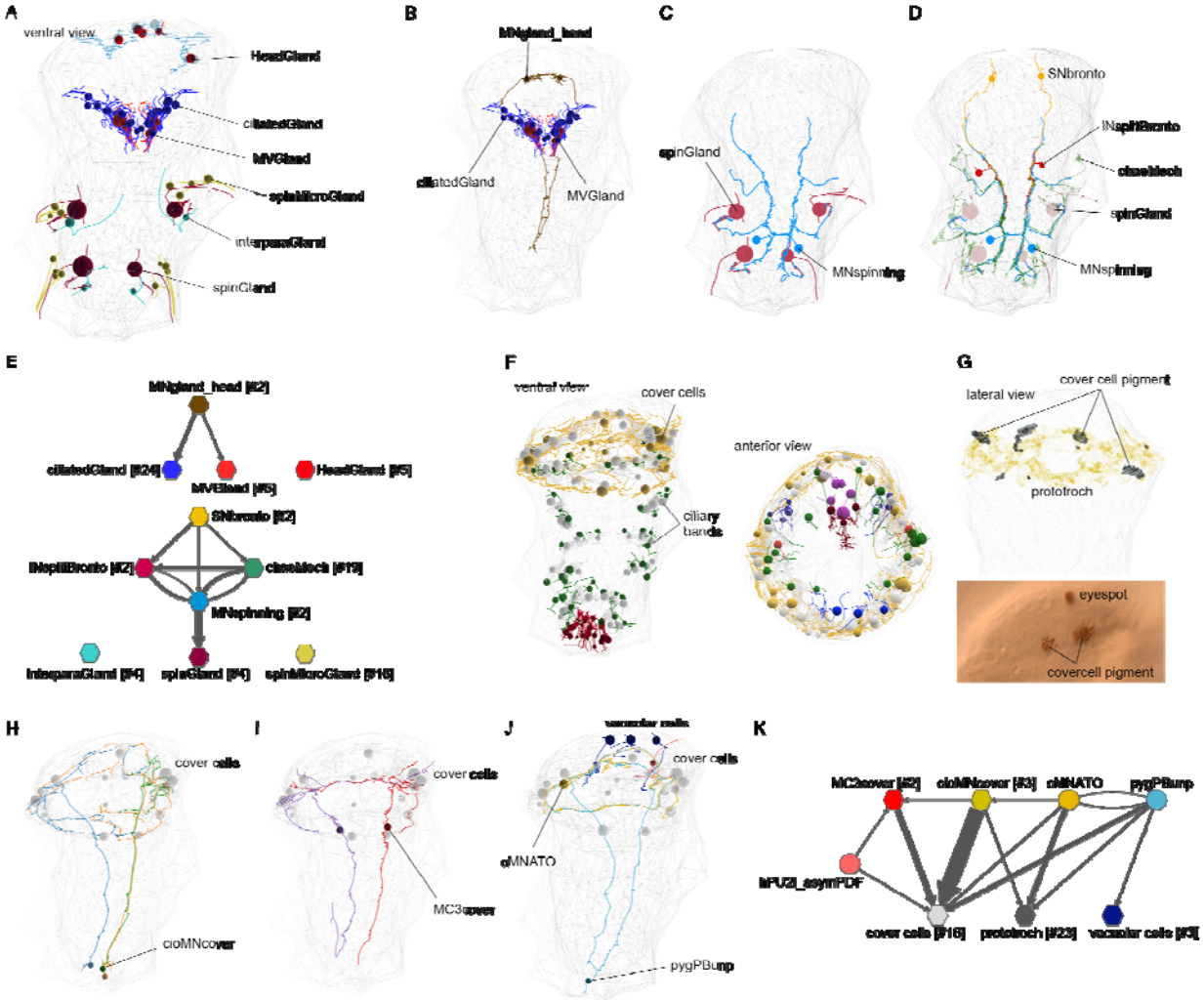

Figure 8. Exocrine glands and pigment cells and their innervation.
(A) Overview of the position of all exocrine gland cells in the EM volume. (B) EM reconstruction of the two MNgland_head motoneurons innervating the ciliatedGland and MVgland cells. (C) EM reconstruction of the two MNspinning motoneurons innervating the four spinGland cells. (D) EM reconstruction of selected input neurons to the MNspinning cells. (E) Network view of the exocrine gland synaptic circuits. Nodes represent groups of neurons, edges represent synaptic connections. Numbers in square brackets indicate the number of cells. The headGland, interparaGlands and spinMicroGland cells receive no synaptic input. (F) Overview of the position of all pigmented cells in the EM volume, ventral and anterior views. (G) Reconstructed cover cells in the EM volume (top) and in a live larva in a DIC image (bottom) showing the position of pigment granules in the cover cell. (H) Reconstruction of the cioMNcover cells. (I) The MC3cover cells. (J) The pygPBunp cells and their postsynaptic partners, the cover cells and the head vacuolar cells. (K) Network view of the pigment cell synaptic circuits. Nodes represent groups of neurons, edges represent synaptic connections.

Pigment cells and their innervation

The second type of non-locomotor effector cells comprises various pigmented epithelial cell types (Figure 8 – figure supplement 2). We distinguished seven pigmented cell types, three of them under neuronal control.

The largest and most densely innervated pigmented cells are the cover cells (16 cells). These form two rows anterior and posterior to the prototroch ciliary band. The cover cells receive synaptic innervation from three groups of neurons with global reach. The largest number of synapses are provided by three pygidial neurons (cioMNcover) with axons reaching the head. The cioMNcover

axons form a double ring around the prototroch, innervating the cover cells both above and below the ciliary band (Figure 8H). The unpaired mechanosensory-pigment-motor pygPBunp neuron projects in a single ring around the cover cells and also synapse on the cover cells. The third pigment-motor cell type is the biaxonal MC3cover neuron with its soma in the first segment (2 cells). This cell has branched axons with smaller branches in between the cover cells that terminate near the cuticle. MC3cover cells are postsynaptic to the SNbronto, SNblunt and SNFVa putative mechanosensory neurons.

All other ciliary band cells are flanked by a different pigment-cell type, the CB pigment cells (58 cells). These cells contain pigment vacuoles with an average diameter of 0.34 µm (stdev=0.08, N=44). In the pygidium, there is a ring of 26 pigmented cells with larger pigment vacuoles (diameter=0.55 µm, stdev=0.14, N=47). In the head, there are three vacuolar cells with brighter vacuolar content. These cells also receive synapses from the pygPBunp neuron. The eyespots and adult eyes also have distinct types of shading pigment cells, with no synaptic partners (Jékely et al., 2008; Randel et al., 2013; Rhode, 1992).

Chaetal mechanoreceptors and their circuits

A prominent trunk mechanosensory system with a high level of connectivity is the circuit of chaetal mechanoreceptors (chaeMech). The chaeMech neurons are dendritic sensory cells found in segments 1-3 in both the dorsal (notopodium) and ventral (neuropodium) lobes of the parapodia. Their sensory dendrites branch between the chaetal sacs and their axon projects to the nerve cord (Figure 9A-C). The sensory dendrites may sense the displacement of the chaetae during crawling (proprioception) or due to external mechanical stimuli. The annelids *Harmothoë* (a polynoid) and *Nereis* have cells with a similar morphology called bristle receptors. These cells show rapidly adapting spikes upon the displacement of the chaetae (Horridge, 1963); (Dorsett, 1964). The chaeMech cells are also similar to dendritic proprioceptors in *Drosophila* larvae that sense body-wall deformations and provide feedback about body position through premotor neurons (He et al., 2019; Vaadia et al., 2019; Zarin et al., 2019).

In *Harmothoë* and *Nereis*, the bristle receptors connect to the giant axon system. The *Platynereis* chaeMech neurons are highly interconnected. They form some of the strongest edges in the connectome (Supplementary table 1) and have the highest number of direct postsynaptic targets (Figure 9D-E; Figure 5A, C). These include the premotor interneurons INsplitCR, INsplitBronto, INchaeMech and the MNring and MNspinning motoneurons. Some trunk PU and CR mechanoreceptors (Bezares-Calderón et al., 2018) are presynaptic to chaeMechs, suggesting a crosstalk between different mechanosensory modalities. The INsplitCR interneurons receive the largest fraction of chaeMech synapses (Figure 5E). INsplitCRs are also postsynaptic to the collar receptors (CR) that mediate a hydrodynamic startle response characterised by parapodial extension and chaetal opening (Bezares-Calderón et al., 2018). This wiring suggests that during a startle, proprioceptive feedback into INsplits by chaeMech cells may regulate the response.

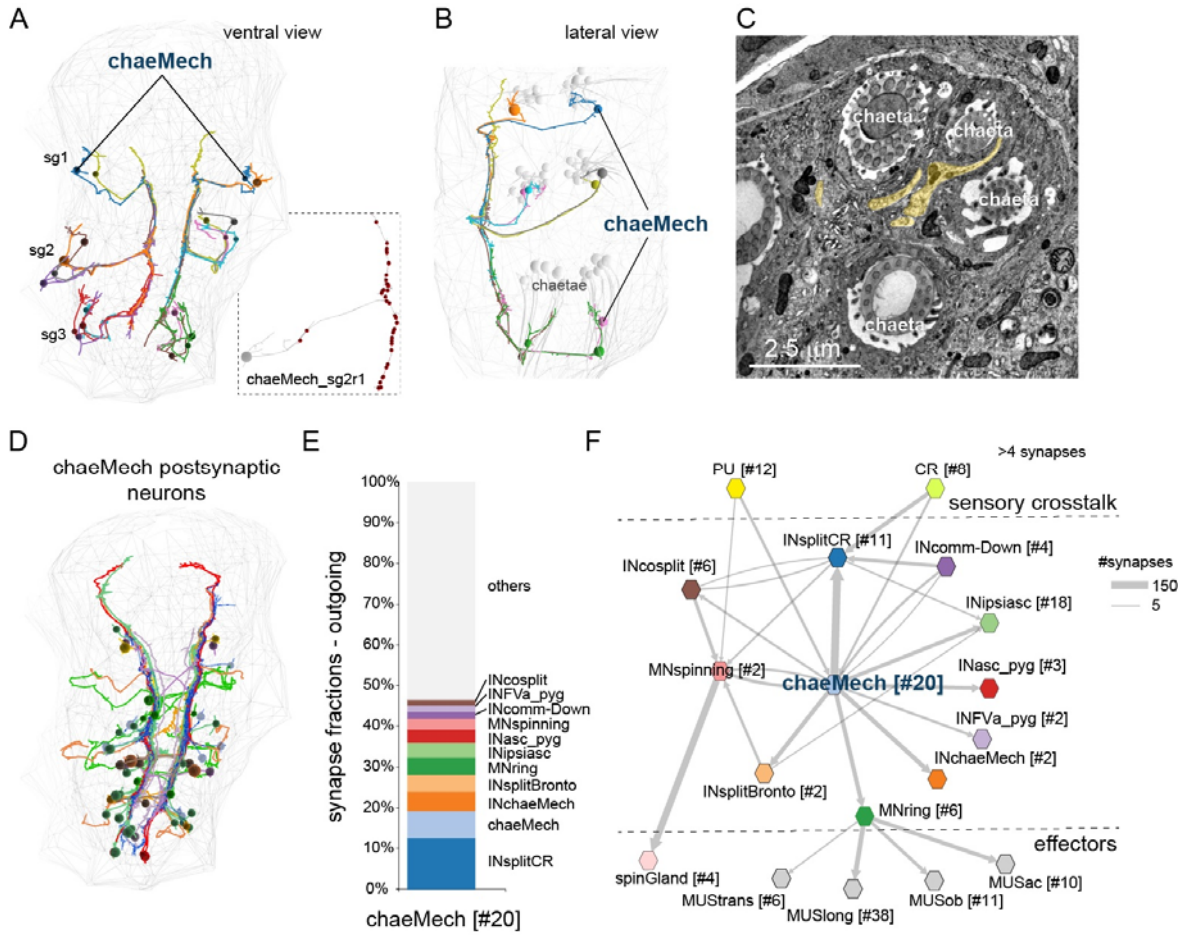

Figure 9. Chaetal mechanoreceptors and their circuits. (A) Skeletons of chaeMech cells in segments 1-3. Inset shows the pseudounipolar morphology of one of the cells. Red dots indicate presynaptic sites. (B) Lateral view of chaeMech cells. The branched dendritic endings run in between the chaetae in the chaetal sacs. (C) TEM image of a chaetal sac with cross-sections of chaetae and chaeMech dendrites (highlighted in yellow). (D) Skeletons of the main postsynaptic targets of chaeMech cells. (E) Fraction of outgoing synapses of chaeMech cells to their main postsynaptic partners. (F) Grouped connectivity graph of chaeMech cells. Nodes represent groups of cells, arrows represent synaptic connections. Edge width shown as the square root of synaptic count.

Mechanosensory circuits and circuit evolution by duplication

The various mechanosensory systems across the body show similarities in their cellular complements and anatomy (Figure 10). There are several mechanosensory cell types in *Platynereis* larvae, as supported by various lines of evidence. Collar receptor (CR) neurons have a penetrating sensory cilium surrounded by a collar of 10 microvilli. CR neurons express the polycystins *PKD1-1* and *PKD2-1*, and detect water-borne vibrations. PB (penetrating biciliated) neurons have two penetrating cilia with a collar and express *PKD2-1* but not *PKD1-1* (Bezares-Calderón et al., 2018)(Figure 10A, B). PU (penetrating uniciliated) neurons have one penetrating sensory cilium surrounded by a collar. These neurons express the mechanosensory channel *NompC* (LABC and GJ, unpublished). InterparaPM (penetrating multiciliary) neurons have 3-4 penetrating cilia, suggesting that they are also mechanosensory (Figure 10A, B). The chaeMech cells are dendritic chaetal mechanoreceptors (Figure 9A-C).

The strongest postsynaptic partners for all these mechanoreceptors are ipsilateral interneurons with a similar bifurcating axon. These interneurons – collectively referred to as INsplit – have several

distinct types (INsplitCR, INsplitPB, INsplitPBant, INsplitPB_RF/Ya, INsplitPUh, INsplitBronto, INCM)(Figure 10C-E). INsplit neurons occur in all four trunk segments and in the head (INsplitPUh) and their distinct types have unique synaptic connectivity. PB and interparaPM neurons specifically target INsplitPB and represent their main input. The dendritic chaeMech and SNbronto neurons both synapse on the INsplitBronto interneurons, which have no other major presynaptic partners. CR neurons synapse on INsplitCR and INCM. ChaeMech cells also strongly target INsplitCR. Some head PU neurons synapse on INsplitPUh.
The repeated pairing of distinct mechanoreceptor cell types with distinct INsplit types suggests an evolutionary pathway for these systems by circuit duplication and divergence.

The mechanosensory girdle

The mechanosensory circuits in the larva collectively outline an anatomical system that we call the mechanosensory girdle. The girdle is characterised by a circular axonal track with a dorsal loop in the brain neuropil and two axon bundles along the trunk ventral nerve cord (VNC), connected at the circumesophageal nerve (Figure 10F, Video 3). The global projections of two INsplit types – INsplitPBant and INsplitPB_RF/Ya – outline the axon tracks of the mechanosensory girdle (Figure 10F). The projections of several other neurons follow this axonal track and form a bundle at the ventral side of the VNC (Figure 10F). The projections of the CR, PB, PU, interparaPM, chaeMech sensory neurons and of all INsplit interneurons run along the mechanosensory girdle, suggesting a separate VNC track for the processing of mechanosensory signals. Searching for pre- and postsynaptic partners for all these neurons we identified further neurons that are part of this system. These include four further sensory cell types, the head SNbronto (dendritic) and SNblunt neurons (blunt sensory ending beneath the cuticle, no cilium) and two pygidial cell types, SNPDF_pyg and SNpygM (Figure 10 – figure supplement 1). Additional interneuron types that join the girdle are the pygidial ascending INasc_pyg (Figure 4D) and the head descending INrope neurons (Bezares-Calderón et al., 2018). The ciliomotor neurons MNant (Verasztó et al., 2017a) and the cover cell motoneurons MC3cover (Figure 5E) are also part of the mechanosensory girdle.
This anatomy and the shared circuitry suggest that the various mechanosensory modalities are integrated by the mechanosensory girdle system. Overall, mechanosensory neurons provide input to all effector systems, including muscles, ciliated cells, glands and pigment cells (Figure 10G).

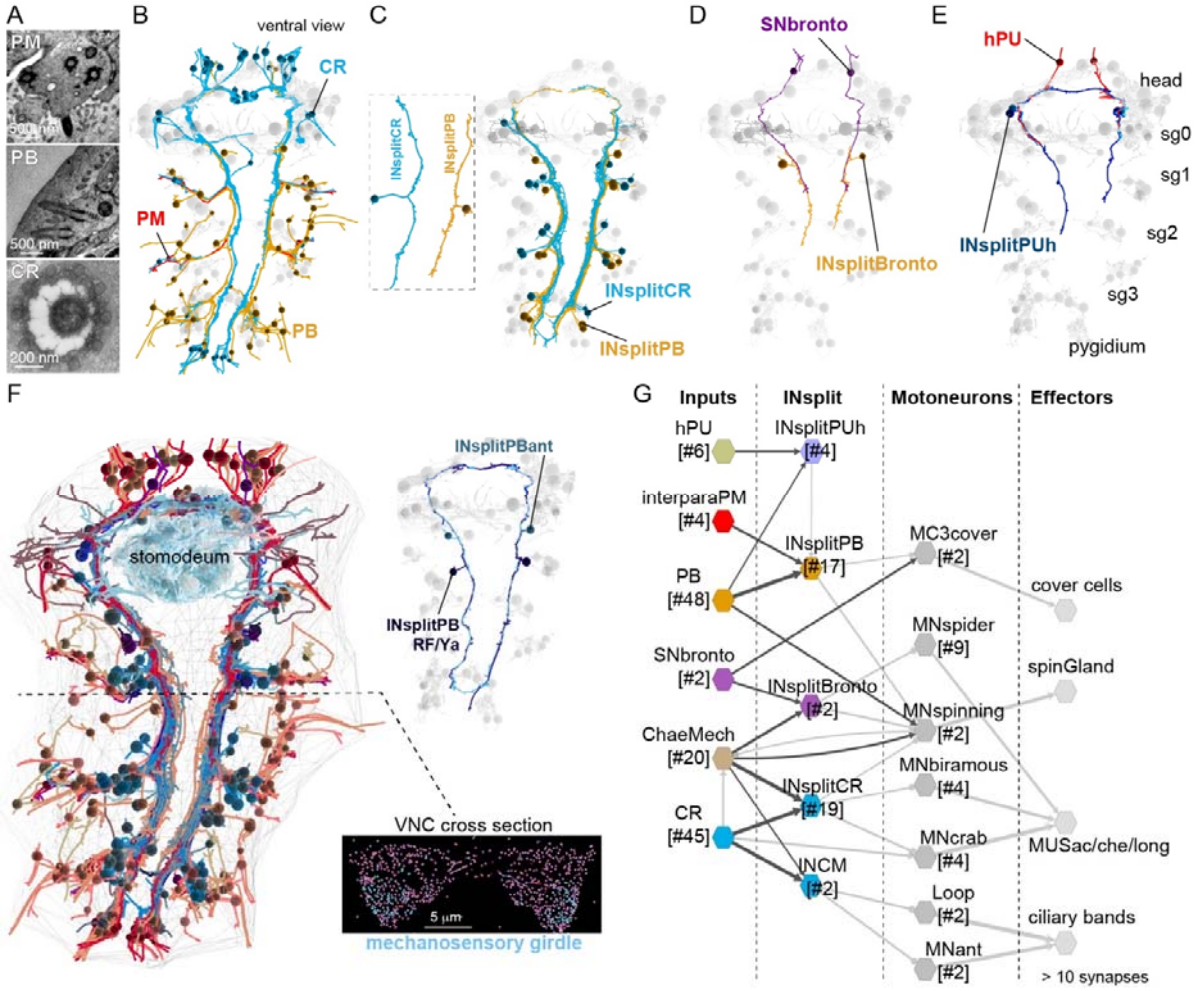

Figure 10. Cells and circuits of the mechanosensory girdle.
(A) TEM images of the sensory endings of interparaPM, PB and CR neurons. (B) Skeletons of CR, PB and interparaPM (PM) neurons. (C) Skeletons of INsplitCR and INsplitPB neurons. (D) Skeletons of SNbronto and INsplitBronto neurons. (E) Skeletons of INsplitPUh and two hPU neurons. (F) Skeletons of all neurons projecting into the mechanosensory girdle. Upper inset: the INsplitPBant and INsplitPB_RF/Ya neurons outline the mechanosensory girdle. Lower inset: cross-section of the ventral nerve cord (VNC) indicating the position of neurites of the girdle (cyan). (G) Synaptic connectivity graph of the main sensory and interneuron types of the mechanosensory girdle. Their main motoneuron targets and effector systems are also shown. Edges represent synaptic connections, nodes represent groups of cells.

Discussion

The *Platynereis* larval connectome and cell-type atlas

The *Platynereis* three-day-old larva connectome is the third and currently largest whole-body connectome, after those of *Caenorhabditis elegans* and the *Ciona intestinalis* larva (Cook et al., 2019; Ryan et al., 2016; White et al., 1986). To facilitate the browsing and querying of the *Platynereis* connectome, the entire dataset – including EM images, skeletons, tags, connectors and annotations – will be available at https://catmaid.jekelylab.ex.ac.uk. We also provide R scripts for data retrieval from the CATMAID server by libraries in the `natverse` toolkit.

The connectome will allow the generation of specific circuit-level hypotheses about neuronal control in the *Platynereis* larva. For example, it suggests that mechanosensory circuits regulate exocrine

glands and pigments cells. We also identified several potential cases of multisensory integration. For example, the eyespot R1 and adult eye photoreceptors converge on the INR1 interneurons suggesting the integration of directional light sensing between the ventral eyespots and dorsal adult eyes.

The EM volume also allowed us to classify all neuronal and non-neuronal cells into 270 types. It will be interesting to compare this morphology and connectivity-based classification to single-cell RNAseq-based classifications. We expect a similar number of molecular types, as suggested by the already available molecular data for *Platynereis (Achim et al., 2015)*, and also by the similar number of morphological and molecular cell types in both the *Ciona* larva and *Caenorhabditis elegans* (Cao et al., 2019; Hobert et al., 2016).

Limitations of the connectome

There are several limitations of connectomics. In *Platynereis*, for example, we know the neurotransmitter or neuromodulator content only of a small fraction of neurons (Figure 4) as these molecules are invisible to EM. However, artificial convolutional neural networks were recently used to predict synaptic transmitter content in the *Drosophila* adult brain from EM images alone (Eckstein et al., 2020). This approach still has to be tested in other organisms including *Platynereis*. An alternative is to register cellular-resolution gene-expression atlases to EM volumes, as has recently been done for six-day-old *Platynereis* (Vergara et al., 2020). The mapping of neurotransmitter-synthesis enzymes or transporters could then reveal transmitter content in single neurons. This is now feasible in *Platynereis* larvae but will require the acquisition of new synaptic-resolution EM volumes. We attempted but could not register the current volume to a three-day-old gene expression map (Asadulina et al., 2012) due to differences in fixation and alignment artefacts.

Another approach to map transmitters and modulators in small and stereotypical nervous systems is to correlate transgenically labelled neurons to EM reconstructions, an approach extensively used in *C. elegans* (Bentley et al., 2016) and also possible in *Platynereis* larvae (Bezares-Calderón et al., 2018; Verasztó et al., 2017a). Alternatively, we have used direct immunogold labelling on sparse sections from the EM series to directly map neuropeptides to the connectome (Shahidi et al., 2015)(Figure 4).

Another limitation of the *Platynereis* connectome is the difficulty to predict sensory-cell function based on ultrastructure alone. We identified 45 sensory neuron types in the larva based on morphology and connectivity, but only know the sensory function of a few of these (Williams and Jékely, 2019). However, it is now possible to combine genetics, behaviour and neuronal activity imaging in *Platynereis* to functionally characterise sensory cell types. Recent work has identified larval UV photoreceptors (Verasztó et al., 2018), hydrodynamic vibration detectors (Bezares-Calderón et al., 2018), chemosensory neurons (Chartier et al., 2018), or the Go-opsin1-expressing shadow detectors in sensory appendages of adult worms (Ayers et al., 2018). The connectome nevertheless allowed us to identify new types of putative mechanosensory neurons – including the SNblunt, SNFVa and SNbronto cells – based on connectivity and morphology alone (Figure 9).

Circuits for whole-body coordination

Platynereis larvae have segmentally repeated effector organs including ciliary bands, parapodia and glands. The connectome suggests that for each of these effector systems, neurons with axons spanning several segments can ensure intersegmental coordination.

Several motoneurons innervate target cells in multiple segments. The two MNspinning neurons innervate the four spinning glands in segments 2-3 with each MNspinning connecting to two glands on the contralateral body side (Figure 8C). Among the muscle motoneurons, MNspider cells synapse on contralateral muscles in two consecutive segments. The muscle targets of MNcrab and MNbow neurons span three segments (Bezares-Calderón et al., 2018). In the pigment-motor

system, the cioMNcover cells each innervate half the ring of the cover cells and pygPBunp innervates the entire ring, suggesting coordinated regulation. The ciliomotor system is characterised by large motoneurons coordinating entire ciliary bands across all segments (Verasztó et al., 2017a). These intersegmental motor systems likely mediate behaviours including the simultaneous recruitment of multiple effectors. Those behaviours that involve intersegmental phase lags such as parapodial crawling (not fully developed at three days) may be mediated by segment-intrinsic motoneurons (e.g. MNantacic, MNpostacic, MNpostv).
Intersegmental coordination is also apparent at the level of sensory and interneurons. For example, individual chaeMech cells can synapse on interneurons in three segments. INrope and INchaeMech interneurons target motoneurons across three segments, INsplitCRATO, INsplitBronto and INsplitVent in two segments. The globally reaching INsplitPBant cells have postsynaptic partners in all four segments and the pygidium.
These examples demonstrate the importance of a whole-body approach in connectomics for the identification of such long-range connections.

Circuit evolution by duplication and divergence

The connectome suggests a model for the evolution of circuits by the duplication and divergence of circuit modules of synaptically connected cell types (Tosches, 2017). This was most apparent in the mechanosensory system where several morphologically similar collared ciliated mechanosensory neurons (CR, PU, PB, PM) synapse on distinct groups of morphologically similar INsplit types.
The similar morphologies of the mechanosensory cells suggests that these represent sister cell types (Arendt, 2008). Further supporting this, PB, CR and pygPBunp neurons share some of their gene regulatory environment as they all can be labelled by a *PKD2-1* transgene (Bezares-Calderón et al., 2018). The cell-type diversification of mechanoreceptors may have been paralleled by the diversification of the postsynaptic INsplit neurons. The duplication and divergence of entire cell type sets has also been proposed for the evolution of the vertebrate cerebellum (Kebschull et al., 2020). Testing this model in *Platynereis* would require the integration of connectomics and comprehensive gene expression analysis.

Segmental organisation and inferences about the evolution of the annelid body plan

The whole-body connectome allowed us to investigate the segmental organisation of the annelid body. Each larval segment has a distinct neuron-type composition with some unique cell types (Figure 7 – figure supplement 1). Several neuron types occur in multiple segments and those shared between all four trunk segments confirm the serial homology of the cryptic segment with the other three segments (Steinmetz et al., 2011). The pygidium has also been hypothesized to have had a metameric origin based on the presence of a pygidial coelomic cavity and muscles (Starunov et al., 2015). One prediction of this model is that there are neurons or muscles of the same type in the pygidium and the main trunk segments. We identified four neuronal (trunk PB, INipsiasc, trunk CR and PU) and two muscle types (MNlong_V, MNtrans) showing this pattern (Figure 7), supporting the metamery hypothesis.
The identification of a mechanosensory girdle in *Platynereis* reminded us of another classic hypothesis about bilaterian body plan evolution, the amphistomy theory. In 1884, Sedgwick suggested that at the origin of bilaterians, a gastric slit in a radially symmetric animal evolved into the mouth and anus through the fusion of the lateral lips (Sedgwick, 1884). If there was a nerve concentration around the gastric opening, like in some cnidarians, this could have evolved into the paired nerve chords characteristic of many bilaterians (Nielsen et al., 2018). Accordingly, the mechanosensory cells in the *Platynereis* girdle could correspond to mechanosensory cells around the cnidarian oral opening (e.g. (Singla, 1975)). One prediction of this scenario is the presence of bifurcating mechanosensory interneurons similar to INsplits running in two directions along the oral

opening in cnidarians. This specific neuroanatomical prediction could be tested by connectomics in cnidarians.

Methods

Specimen preparation, transmission electron microscopy and image processing

Fixation and embedding were carried out on an 72 hpf *Platynereis* larva (HT9-4) as described previously (Conzelmann et al., 2013). Serial sectioning and transmission electron microscopy were done as described in (Shahidi et al., 2015). The section statistics for the HT9-4 (NAOMI) specimen were previously described (Randel et al., 2015).
Serial sections were imaged on a FEI TECNAI Spirit transmission electron microscope with an UltraScan 4000 4X4k digital camera using Digital Micrograph acquisition software (Gatan Software Team Inc., Pleasanton) and SerialEM (Schorb et al., 2019). The images for the HT9-4 projects were scanned at various pixel resolutions: 5.7 nm/pixel, 3.7 nm/pixel, and 2.2 nm/pixel. Image stitching and alignment were done in TrakEM2 (Cardona et al., 2012). We used CATMAID for skeleton tracing, reviewing, annotation and connectivity analysis (Saalfeld et al., 2009; Schneider-Mizell et al., 2016).
Due to contrast and focus problems in the main dataset we had to re-image certain layers at higher resolutions, to allow tracing of neurons. These re-imaged series were made into independent CATMAID projects. This included five extra projects, taken at various points throughout the main dataset (Table 4). The largest of these, Plexus_HT-4_Naomi_project__372-4013, consisted of 1407 layers at resolution of 2.2 nm. This stack mostly focused on the brain plexus and the ventral nerve cord where most neurites and synapses occur. Other projects consisted of three jump/gap regions that required not only high resolution but also better realignment. One set contained all the immunogold labelled layers (Shahidi et al., 2015) that were not included in the main aligned dataset. These layers had very low contrast due to the immunolabelling procedure and therefore required higher resolution imaging. All projects were first created and processed in TrakEM2 and then exported as flat jpeg images into CATMAID.

Neuron tracing, synapse annotation and reviewing

To digitally reconstruct every neuron in the serial TEM dataset of the three-day-old larva, we used the collaborative web application CATMAID (Schneider-Mizell et al., 2016) installed on a local server. Ultrastructural features (number and orientation of microtubules, electron density of the cytoplasm and vesicles, ER structure) and a high resolution dataset of the neuropil and the ventral nerve cord aided tracing. At the approximate centre of each nucleus, we changed the radius of a single node according to the soma size in that layer. Skeletons were rooted on the soma and the node was tagged with ‘soma’. We identified synapses based on a vesicle cloud close to the plasma membrane. Most synapses were visible in consecutive layers (for example images see (Randel et al., 2014) and browse the data). We also checked for the proximity of mitochondria in the same arbor in case of an ambiguous synapse – a requirement supported by quantitative connectomic data in *Drosophila* (Schneider-Mizell et al., 2016).
The systematic review of all neurons belonging to a cell type was done by one or multiple reviewers until close to 100% was reached for every cell. Cells were further checked in the 3D widget to split implausible skeletons. Synapses were reviewed multiple times, from both the pre- and postsynaptic arbor.

Cell nomenclature and annotations

All cells have a unique name. We named neurons based on their type (e.g. sensory or motor) cell body position (left or right, head or trunk segment), axonal morphology, neuropeptide expression, and other specialisations (e.g. sensory morphology). Cells of the same type have similar names, distinguished by body position indicators and numbers (Tables 1 and 2). We endeavoured to give names that were easy to remember. The name of many sensory neurons start with SN followed by a specific term (e.g. blunt, bronto, stiff). Interneurons often start with IN and motoneurons with MN. There are exceptions, including neurons with known function (e.g. PRC for photoreceptor cells) and neurons with prominent morphology (e.g. Loop). Segmental position (sg0-3) and body side (l or r) is indicated in the name of most neurons. Non-neuronal cells were named based on anatomical terms (e.g. prototroch) or by abbreviations (e.g. EC for epithelial cell).
All cells have multiple annotations, which can be used to query the database in CATMAID or in the `natverse`. Neurons belonging to a cell type category were annotated with the generalist annotation 'celltype' and a cell-type-specific annotation (e.g. celltype23 for the INpreMN neurons). Non-neuronal cells belonging to a cell type category were annotated with the generalist annotation 'celltype_non_neuronal' and a cell-type-specific annotation (e.g. celltype_non_neuronal23 for the acicula cells). Neurons were also annotated with descriptors of their projection morphologies (e.g. commissural, ipsilateral, pseudounipolar etc.), neuron class (Sensory neuron, sensory-motor neuron, sensory-neurosecretory neuron, interneuron, inter-motorneuron and motorneuron [note the 'r']) as defined earlier (Williams and Jékely, 2019). In CATMAID, we recommend the use of regular expressions for searching annotations e.g. ^motorneuron$ to retrieve exact matches. Differentiating neurons with immature sensory dendrites or axonal projections with axonal growth cones and with no or few synapses were annotated 'immature neuron' (389 cells). Ascending trunk neurons and descending head neurons traversing the circumesophageal connectives were annotated 'head-trunk'. Neurons with a soma in the head and a descending decussating axon were annotated with 'decussating'. Cells were also annotated according to the location of their soma in a certain body region (head – as 'episphere', trunk – as 'torso', 'pygidium'), body side ('left_side', 'right_side'), segment ('segment_0' etc.), and germ layer (ecto-, meso-, endoderm).

Criteria for including cells in the connectome

We defined the final set of cells that were included in the connectome based on the number of incoming and outgoing synapses per cell. First, we selected all cells with a soma (8,852). Next, we removed all cells without a synaptic partner with a soma, resulting in 3,332 cells. We further removed cells with <3 outgoing synapses and no incoming synapse (weighted in-degree=0, weighted out-degree<3), except sensory neurons and neurons that belonged to a cell type with other well-connected members. We also removed cells with no outgoing synapses and <3 incoming synapses (weighted in-degree<3, weighted out-degree=0), except effector cells and neurons that belonged to a cell type with other well-connected members. The removed cells are 'dead ends' and unless they are sensory cells with output or effector cells with input, will not contribute to global connectivity. We also removed small clusters of only locally connected neurons. This resulted in a set of 2,728 cells (Catmaid annotation 'connectome'; Figure1 – source data 1).

Network analysis, NBLAST and Sholl analysis

We used CATMAID (several releases), Gephi 0.9.2 and Python for network analysis. To detect communities, we used Gephi with the 'modularity' function, considering edge weights and randomisation.
NBLAST was carried out in the `natverse` (Bates et al., 2020; Costa et al., 2016) by a custom R script. We compared 1,772 neurons in the connectome (annotated: "connectome_neuron"). First,

skeletons were imported from the Catmaid database to R with the 'read.neurons.catmaid' command. Skeletons were smoothed by 'smooth_neuron' with a sigma of 6000. Skeletons were converted to point vector format by 'dotprops'. We calculated all by all NBLAST scores by 'nblast_allbyall' (version 1) and clustered the results with 'nhclust' with the 'ward.D2' method. Sholl analysis was done in CATMAID in the 'Morphology plot' widget (Schneider-Mizell et al., 2016). We used a radius of 100 nm and centred the analysis on the root node (soma). The Scholl profiles for the 772 connectome neurons were exported as a .csv file and analysed in R. Pairwise distances were calculated with the 'minkowski' method and the distance matrix was clustered with the 'ward.D2' method. The dendrogram was plotted with the 'dendextend' library. The dendrogram based on connectivity was calculated from the synaptic matrix of the 1,772 connectome neurons as presynaptic partners (rows) and the connectome cells as postsynaptic partners (columns).

Tables

Neuronal cell types

Name	description	Main presynaptic partners	Main postsynaptic partners	# of cells	Catmaid annotation	reference
PRC	Rhabdomeric photoreceptor of the adult eye in the head	None	IN1	24	celltype1	(Randel et al., 2015, 2014)
IN1	First order visual interneuron	PRC	INton	4 + 7 weakly connected (INint)	celltype2	(Randel et al., 2015, 2014)
INton	Trans-optic-neuropil interneuron, eye circuit	IN1	INsn	4	celltype3	(Randel et al., 2015, 2014)
INpreSer	Head interneuron		Ser-h, INarc1	2	celltype4	this study
cPRC	Ciliary photoreceptor, head		INRGW, INNOS, neurosecretory	4	celltype5	(Verasztó et al., 2018; Williams et al., 2017)
INRGW	RGW interneuron, head, peptidergic	cPRC, INRGW	Ser-h, neurosecretory	4	celltype6	(Verasztó et al., 2018; Williams et al., 2017)
INNOS	RGW interneuron, head, peptidergic	cPRC	INRGW, neurosecretory	4	celltype7	(Verasztó et al., 2018; Williams et al., 2017)
Ser-h1	Serotonergic ciliomotor neuron	INRGW	Prototroch ciliary band	2	celltype8	(Verasztó et al., 2017a)
MC	Ciliomotor neuron		Prototroch ciliary band	1	celltype9	(Verasztó et al., 2018)
cMNPDF-vcl1	Ciliomotor neuron, possible pacemaker neuron	Ser-h1, cMNATO, cMNdc	cMNATO, cMNdc, prototroch, Ser-h1, pygPBunp,	1	celltype10	(Verasztó et al., 2018)

			MC, INRGW			
cMNATO	Ciliomotor neuron, possible pacemaker neuron	SNbicil, cMNPDF-vcl1, Ser-h1, pygPBunp	MC, SN, cMNdc, pygPBunp, prototroch, Ser-h1, Loop,	1	celltype11	(Verasztó et al., 2017a)
cMNdc	Ciliomotor neuron, possible pacemaker neuron	cMNPDF-vcl1, cMNATO	INarc1, MNant, pybPBunp, prototroch, MC	1	celltype12	(Verasztó et al., 2017a)
SNnuch	Nuchal organ sensory neuron, peptidergic (PDF)	SN_DSO10, SNnuch	INarc, SNnuch	22	celltype13	(Shahidi et al., 2015)
SNnuch NS	Neurosecretory nuchal organ sensory neuron		neurosecretory	3	celltype14	(Williams et al., 2017)
SNnuchBx	Nuchal organ sensory neuron		INbiax	2	celltype15	this study
SN_LHSO2golden	Sensory neuron in lateral head sensory organ 2		SN_DLSO1	2	celltype16	this study
SNhorn	Sensory neuron, head, adjacent to eyespot		MNant	2	celltype17	this study
SNhook	Sensory neuron, head		MNant, INdecussHook	2	celltype18	this study
MNant	Biaxonal ciliomotor neuron, head	SNantlerPDF, SNhook, INCM_sg1, cMNdc, Ser-tr	Metatroch, prototroch, paratrochs	2	celltype19	(Verasztó et al., 2017a)
SNIasso	Sensory neuron, head		INIasso_preSN, INRGW, INW	2	celltype20	this study
INIasso	Head interneuron	SNIasso, INIasso	INsn, INpreMN, INIasso	9	celltype21	this study
INdecussPre	Head decussating interneuron	INpreMN, INsn_like		2	celltype22	this study
INpreMN	Head interneuron	INIasso, INRGW	Ventral head MNs	6	celltype23	(Verasztó et al., 2018)
SNMIP-vc	MIP sensory neuron, head		MNr3, neurosecretory	2	celltype24	(Shahidi et al., 2015)
SNmus	Sensory neuron, head		**INmus** (weak)	2	celltype25	this study
SNantlerPDF	PDF sensory neuron, head		MNr3, MNl3, MNant, INhook	2	celltype26	this study
SNPDF-dc	PDF sensory neuron, head, dorsolateral sense organ 1		SN_DLSO1.3_2	2	celltype27	(Shahidi et al., 2015)
SN_DLSO1.2_4	PDF sensory neuron, head, dorsolateral sense		neurosecretory	2	celltype28	(Shahidi et al., 2015)(Williams et al., 2017)

	organ 1, neurosecretory plexus					
SN_DLSO1	Sensory neuron, head dorsolateral sense organ 1	SN_DLSO	neurosecretory	29	celltype29	(Williams et al., 2017)
SN_DLSO1.2_1	Sensory neuron, head dorsolateral sense organ 1.2	SN_LHSO2golden		2	celltype30	
SN_DLSO2	Sensory neuron, head dorsolateral sense organ 2	SN_DLSO1	SN_DLSO1	12	celltype31	this study
SN_LHSO2	Sensory neuron, lateral head sense organ 2		SN_DLSO		celltype32	
eyespot_PRC_R3	Rhabdomeric opsin3-expressing eyespot photoreceptor		Lateral prototroch cells, ventral MN	2	celltype33	(Jékely et al., 2008; Randel et al., 2013)
eyespot_PRC_R1	Rhabdomeric opsin1-expressing eyespot photoreceptor		INR1, SN_DLSO1.1, INR1	2	celltype34	(Randel et al., 2013)
MS1	MS penetrating mechanosensory cell – type 1, median head	INpreMN, INRGW	vMN,	1	celltype35	(Bezares-Calderón et al., 2018; Verasztó et al., 2018)
MS2, MS4	MS penetrating mechanosensory cell – type 2, asymmetric	INRGW, MS2-4	vMN	2	celltype36	(Bezares-Calderón et al., 2018; Verasztó et al., 2018)
MS3	MS penetrating mechanosensory cell – type3		INCrossbow	2	celltype37	(Bezares-Calderón et al., 2018; Verasztó et al., 2018)
MS5	MS penetrating mechanosensory cell – type4	INsn	vMN	2	celltype38	(Bezares-Calderón et al., 2018; Verasztó et al., 2018)
SN-ASTC1	allatostatinC-expressing sensory-neurosecretory neuron, head apical organ	cPRC	cPRC, SN_MIP1, neurosecretory	2	celltype39	(Williams et al., 2017)
SN_DLSO3PDF	Head sensory neuron, dorsolateral sensory organ 3, PDF expressing	cMNATO		2	celltype40	
INDLSO	Head interneuron	SN_DLSO	INarc1, INUturn2	2	celltype41	this study
MC2biax	Head biaxonal	-	-	2	celltype42	this study

	neuron					
SN_IRP2_burs	Insulin-like peptide 2 and bursicon expressing sensory-neurosecretory neuron, head apical organ		neurosecretory	1	celltype43	(Williams et al., 2017)
SN_IRP2_FMRF	Insulin-like peptide 2 and FMRFa expressing sensory-neurosecretory neuron, head apical organ		neurosecretory	1	celltype44	(Williams et al., 2017)
SN_MIP4	MIP-expressing sensory-neurosecretory neuron, head apical organ		neurosecretory	2	celltype45	(Williams et al., 2017)
SN_MIP1	MIP-expressing sensory-neurosecretory neuron, head apical organ	cPRC	neurosecretory	2	celltype46	(Williams et al., 2017)
MNspinning	spinGland motoneuron, segment 2	chaeMech, INsplitBronto, INsplitCR, spinPB, INbiaxH	spinGland, chaeMech	2	celltype47	this study
SN_WLD	WLD neuropeptide-expressing sensory-neurosecretory neuron, head apical organ	SN_NS3r, SN_DLSO	neurosecretory		celltype48	(Williams et al., 2017)
SN_DSO	Sensory neuron, dorsal head sensory organ	SN_DSO	SNnuch, SN_DSO	17	celltype49	this study
SNbicil	Biciliated sensory neuron, ventral head	cMNATO	cMNATO	2	celltype50	this study
SNasym	Biciliated sensory neuron, head apical organ, asymmetric		INarc2, INasym	1	celltype51	this study
SN47Ach	Achatin-expressing sensory neuron, head apical organ, asymmetric		INRGW, INUturn, neurosecretory	1	celltype52	(Williams et al., 2017)
INcrossbow	Head interneuron	MS3, INRGW, SNasym		2	celltype53	this study
pygPBunp	Biciliated penetrating sensory neuron, biaxonal, pygidium	cMNATO, cMNdc, cMNPDF-vcl1, Ser-h1,	Cover cells, MC, Ser-h1, vacuolar_cell_head, prototroch	1	celltype54	(Bezares-Calderón et al., 2018; Shahidi et al., 2015; Verasztó et al.,

						2017a)
INarc1	Interneuron, head	SNnuch, cMNdc, pygPBunp	vMN	2	celltype55	(Randel et al., 2015)
INarc2	Biaxonal interneuron, head	SNnuch, SNasym, Ser-h1, cMNATO	cMNATO	2	celltype56	(Randel et al., 2015)
INsn	Head Schnörkel interneuron	INlasso_postSN, INRGW, INton, INsn	vMN, INpro, INproT2, INsn, MS5	6	celltype57	(Randel et al., 2015, 2014)
INrope	Descending head interneuron	SNbronto, head collar receptors (CR), Loop	Loop, MNsmile, MNspider, MNbiramous	2	celltype58	(Bezares-Calderón et al., 2018)
Loop	Intersegmental ciliomotor neuron, segment 1	INCM, INrope, Ser-tr1, cMNATO, MNant	Multiciliated cells, MNant, Ser-tr1	2	celltype59	(Bezares-Calderón et al., 2018)
INCM	Pseudounipolar interneuron, segment 1	Head collar receptors (CR), chaeMech	Loop, MNant	2	celltype60	(Bezares-Calderón et al., 2018)
MNspider	Motoneuron, segments 2,3	INrope, INsplitBronto, INipsiasc	MUSac, MUSchae, MUSob, MUSlong	8	celltype61	(Bezares-Calderón et al., 2018)
MNsmile	Motoneuron, segment 1	INrope	MUSmouth, MUStrans, MUSax, MUSlong	8	celltype62	(Bezares-Calderón et al., 2018)
MNbiramous	Motoneuron, segments 1,2,3	INrope, INspiltCR, INleucoPU	MUSchae	6	celltype63	(Bezares-Calderón et al., 2018)
MNring	Motoneuron, segments 1,2,3 and pygidium	INrope, INATO_pyg, chaeMech, Ser-tr1	MUSlong, MUSac, MUSchae, MUStrans, MUSob	32	celltype64	(Bezares-Calderón et al., 2018)
MNcrab	Motoneuron, segments 2,3	INsplitCR, collar receptors (CR), pygPBunp	MUSchae, MUSac, MUSlong, MUSob, MUSmouth	4	celltype65	(Bezares-Calderón et al., 2018)
MNhose	Motoneuron, segments 1,2,3	INrope, INleucoPU, chaeMech	MUStrans, MUSob-post, MUSob-ant	6	celltype66	(Bezares-Calderón et al., 2018)
MNbow	Motoneuron, segment 2, enkephalin positive	INcosplit, INsplit	MUSac, MUSchae, MNbiramous	2	celltype67	(Bezares-Calderón et al., 2018)
MNwave	Motoneuron, segments 2,3	INleucoPU, INsplitCR	MUSac, MUSchae	6	celltype68	(Bezares-Calderón et al., 2018)
MNacicX	Motoneuron, segments 2,3	MNpostv, INchaeMech	MUSac, MUSchae, MUSlong	3	celltype69	this study

INchaeMech	Premotor interneuron, segment 3	chaeMech	MNacicX, MNspider	2	celltype70	this study
chaeMech	Bristle (chaetal) dendritic mechanoreceptor	MNspinning, chaeMech	INsplitCR, INsplitBronto, INchaeMech, MNspinning, MNring, INbiaxH, chaeMech, INasc_pyg, INFVa_pyg	20	celltype71	this study
INFVa_pyg	Pygidial FVamide-positive ascending interneuron	chaeMech	MNladder	2	celltype72	(Shahidi et al., 2015)
INsplitCR	Pseudopolar ipsilateral interneuron, cryptic segment, segments 1-3	Collar receptors (CR), chaeMech, INcomm-DownL, INbiaxH	MNcrab, MNbiramous, MNwave, MNspinning	17	celltype73	(Bezares-Calderón et al., 2018)
INsplitCRATO	Pseudopolar ipsilateral interneuron, segment 3	Collar receptors (CR), chaeMech	MNcrab, MNbiramous, MNspinning, pygidial pigment cells	2	celltype74	(Bezares-Calderón et al., 2018)
INMC3	Head interneuron	PU (weak)	MC3cover, INCM	2	celltype75	this study
INbiax	Head biaxonal descending interneuron	SNnuchBx	INsplit, INbiax, Ser-tr1, INW	2	celltype76	this study
INsplitPB_RF/Ya	Pseudounipolar interneuron, segment 1, PDF and RF/Ya-expressing	PB	INsplitPBant	2	celltype77	this study
INsplitPBant	Pseudounipolar interneuron, segment 1, PDF and RYa-expressing	PB, INsplitPB_RF/Ya	INasc_pyg, INsplitPUh, SNPDF_pyg	2	celltype78	this study
INsplitPB	Pseudounipolar interneuron, segments 1,2,3	PB, INsplitPB, INsplitPB_RF/Ya, interparapodialPM	INsplitPB, INasc_pyg, INleucoPU, SNPDF_pyg, MNspinning	17	celltype79	this study
PB	Penetrating biciliated mechanosensor, head, segments 1,2,3 and pygidium	PB, INsplitPB	PB, INsplitPB, MNspinning, SNFVa	54	celltype80	this study
interparaPM	Penetrating multiciliated mechanosensor, segments 1,2		INsplitPB	4	celltype81	this study
cioMNcover	Covercell		covercell	3	celltype82	this study

	motoneuron, pygidium					
INheadPU	Head pseudounipolar interneuron	PU	INsplitPBant	3	celltype83	this study
MNl3, MNr3 (vMN3)	Ventral head decussating ciliomotor neuron	MS, INsn, SNantlerPDF, eyespotPRC, INpreMN, SNMIP-vc	prototroch 1,2,3,7,8clock, ventral MN	2	celltype84	(Randel et al., 2015)
MNl1, MNr1 (vMN1)	Ventral head decussating muscle and ciliomotor neuron, ventral projection	MS, INsn, SNantlerPDF, eyespotPRC, INpreMN,	ventral paratroch, ventral MUSlong	2	celltype85	(Randel et al., 2015)
MNl2, MNr2 (vMN2)	Ventral head decussating muscle and ciliomotor neuron, dorsal projection	MS, INsn, SNantlerPDF, eyespotPRC, INpreMN,	dorsal paratroch, dorsal MUSlong	2	celltype86	(Randel et al., 2015)
MC3cover	Covercell motoneuron, biaxonal, segment 1	SNbronto, SNblunt, SNFVa, INMC3, INsplit	Covercell, EC pigmented	2	celltype87	this study
antPUc	penetrating uniciliated sensory neuron, antenna, head		MC	17	celltype88	(Bezares-Calderón et al., 2018)
spinPU	spinGland-adjacent penetrating uniciliated mechanosensor, segments 2,3			9	celltype89	(Bezares-Calderón et al., 2018)
VentraltrunkPUunp-Glialike	trunk penetrating uniciliated mechanosensor		MNgland_head	1	celltype90	this study
Ciliary band PU neurons (ventralParaPU ventralTeloPU dorsalParaPU dorsalTeloPU)	trunk penetrating uniciliated mechanosensor, adjacent to ciliary bands, segments 1,2,3, pygidium		INleucoPU, MNladder	31	celltype91	(Bezares-Calderón et al., 2018)
hPUc1	penetrating uniciliated mechanosensor, head		INCrossbow	2	celltype92	(Bezares-Calderón et al., 2018)
pygCirrusPU_SM	Pygidial sensory-motor neuron, penetrating cilium		MUSlong_pyg	2	celltype93	this study
interparaPU, hCirrusPU	Interparapodial penetrating uniciliated mechanosensor, cryptic segment, segments 1-3			14	celltype94	(Bezares-Calderón et al., 2018)

Parapodial PU (notopodPU, neuropodPU)	parapodial penetrating uniciliated mechanosensor, segments 1,2,3	INleucoPU		26	celltype95	(Bezares-Calderón et al., 2018)
hPU	Head penetrating uniciliated mechanosensor		INsplitPUh	6	celltype96	(Bezares-Calderón et al., 2018)
dsoPU	Head dorsal sense organ penetrating uniciliated mechanosensor, asymmetric		INsplitPUh	4	celltype97	(Bezares-Calderón et al., 2018)
pygCirrusPU	Pygidial cirrus penetrating uniciliated mechanosensor		INbiaxLeg	13	celltype98	(Bezares-Calderón et al., 2018)
hPU2l_asymPDF	Asymmetric head PU neuron, PDF-positive		coverell4clock_ant	1	celltype99	this study
antCR, dsoCR, hCR	Head collar receptor (headCR)		INCM, INrope, INsplitCR, INarc	24	celltype100	(Bezares-Calderón et al., 2018)
pygCirrusCR, ventralpygCR, interparaCR	trunk collar receptor, cryptic segment, segments 1-3, pygidium	pygCirrusCR, ventralpygCR	INsplitCR, MNcrab, pygPBunp, INcomm	21	celltype101	(Bezares-Calderón et al., 2018)
doCRunp	Unpaired dorsal head collar receptor	CR	MNcrab, INCM, INsplitCR	1	celltype102	this study
SN_DLSO1.0_1	Head sensory neuron, dorsolateral sense organ 1	SN_LHSO	SN_DLSO	2	celltype103	this study
INdc	Head dorsal interneuron	INsn	INsn, ventral MN	6	celltype104	(Randel et al., 2015, 2014)
INbackcross	Dorsal trunk interneuron, segments 1,2,3	Loop		6	celltype105	this study
MNmouth	Trunk motoneuron, segment 2	INrope, INleucoPU	MUSmouth	2	celltype106	this study
MNob-ipsi	Trunk motoneuron, segments 2,3		MUSob	4	celltype107	this study
INbiaxLeg	Trunk interneuron, segment 2	PU, CR	INsplitCR	3	celltype108	this study
INbiaxH	Trunk interneuron, segments 1,2	chaeMech	INsplitCR, MNspinning	5	celltype109	this study
SN_NS1	Sensory-neurosecretory neuron, head apical organ	-	-	2	celltype110	(Williams et al., 2017)

SN_NS3	Sensory-neurosecretory neuron, head apical organ	-	SN_WLD	2	celltype111	(Williams et al., 2017)
SN_NS4	Sensory-neurosecretory neuron, head apical organ	-	-	1	celltype112	(Williams et al., 2017)
SN_NS15	Sensory-neurosecretory neuron, head apical organ	SN_NS15	SN_YF5cil	2	celltype113	(Williams et al., 2017)
SNaant	Ventral head sensory neuron		INZ	9	celltype114	this study
SNPDF_pyg	PDF-expressing ascending sensory neuron, pygidium	INsplitPB, SNpygM	SNstiff, INdesc	2	celltype115	this study
INfoot	Head interneuron	-	INdecussfoot	4	celltype116	this study
INW	Head decussating interneuron	SNlasso, INlat, INhook	INUturn	5	celltype117	this study
INmidL	Head interneuron	-	-	4	celltype118	this study
INhook	Head interneuron	SNantlerPDF	INW	2	celltype119	this study
INlat1	Head interneuron		INW	2	celltype120	this study
INlat2	Head interneuron	MS1	INproT2	2	celltype121	this study
INSturn	Head interneuron			2	celltype122	this study
INcross	Head interneuron	INZ, INpro	INpro	9	celltype123	this study
INpro	Head decussating interneuron	INpro, INsn	INpro	12	celltype124	this study
INproT2	Head decussating interneuron	MS1, INpreMN, INsn, INlat	MNring	4	celltype125	this study
INpear	Head interneuron		INbush	4	celltype126	this study
INZ	Head interneuron	SNaant, INZ	INZ, INpro	7	celltype127	this study
MNpostv	Trunk motoneuron, segments 2,3	MNacicX	MNacicX, MUSac-postv	4	celltype128	this study
SN_NS22	Sensory-neurosecretory neuron, head apical organ	-	-	2	celltype129	(Williams et al., 2017)
SN_NS5	Sensory-neurosecretory neuron, head apical organ	-	INRGW	2	celltype130	(Williams et al., 2017)
SN_NS17	Sensory-neurosecretory neuron, head apical organ	-	-	2	celltype131	(Williams et al., 2017)

SN_YF5cil	Sensory-neurosecretory neuron, head apical organ	SN_NS15, SN_NS16	SNnuch_r2	1	celltype132	(Williams et al., 2017)
SN_NS19	Sensory-neurosecretory neuron, head apical organ	cPRC	-	2	celltype133	(Williams et al., 2017)
SN_NS20	Sensory-neurosecretory neuron, head apical organ	cPRC	-	2	celltype134	(Williams et al., 2017)
SN_NS6	Sensory-neurosecretory neuron, head apical organ	-	-	1	celltype135	(Williams et al., 2017)
SN_NS29	Sensory-neurosecretory neuron, head apical organ	-	-	2	celltype136	(Williams et al., 2017)
SN_NS29	Sensory-neurosecretory neuron, head apical organ	-	-	2	celltype137	(Williams et al., 2017)
SN_NS18	Sensory-neurosecretory neuron, head apical organ	-	-	2	celltype138	this study
SN_NS18	Sensory-neurosecretory neuron, head apical organ	-	SNnuch_2r, SN_YF5bicil	2	celltype139	(Williams et al., 2017)
INbigloop	Head interneuron	-	-	4	celltype140	this study
SNadNS22	Head sensory neuron	-	-	2	celltype141	this study
Ser-tr1	Trunk serotonergic ciliomotor neuron, segment 1	Loop, cMNATO, INdesc	Ciliary bands, MNant	2	celltype142	(Verasztó et al., 2017a)
SNFVa	FVamide-positive sensory neuron, segments 2, 3	PB, INsplitPB	MC3cover, INsplitSNFV, MNspinning	SNFVa	celltype143	(Shahidi et al., 2015)
INUturn	Head interneuron	SN47Ach	Ser-tr1	2	celltype144	this study
INATO_pyg	Pygidial interneuron, allatotropin/orexin-positive		INcomm, Ser-tr1	2	celltype145	this study
INcomm-Upstairs	Commissural ascending interneuron, segment 3 and pygidium			11	celltype146	(Bezares-Calderón et al., 2018)
INasc_pyg	Pygidial ascending	chaeMech,		3	celltype147	this study

	interneuron	SNpygM				
SNblunt	Head sensory neuron, blunt sensory ending, no cilium		MC3cover	2	celltype148	this study
INsplitBronto	Pseudounipolar interneuron, segment 1	SNbronto, chaeMaech	MNspinning, MNspider	2	celltype149	this study
INleucoPU	Descending interneuron, leucokinin-positive, segment 1	Parapodial PU, INsplitPB	MNladder, MNwave, MNmouth	2	celltype150	this study
MNladder	Descending motoneuron, segment 1	INleucoPU, INpreLadder, INcommdesc, INFVa-pyg	MUStrans_pyg, MUSob	2	celltype151	this study
INdecussfoot	Decussating head interneuron	INfoot		2	celltype152	this study
INdecusshook	Decussating head interneuron	SNhook, Ser-h1	INcommasc	2	celltype153	this study
INpreLadder	Interneuron, Allatotropin positive, segments 2,3		MNladder	4	celltype154	this study
INcomm-Upcross	Commissural ascending interneuron, segment 2	Collar receptors (CR)	Collar receptors (CR)	7	celltype155	(Bezares-Calderón et al., 2018)
MNacic	Trunk motoneuron, segments 1,3		MUSac, MUSchae	3	celltype156	this study
INsplitVent	Trunk interneuron, segment 2	INrope	INsplit, MNring	2	celltype157	this study
INcomm-Down	Commissural descending interneuron	Collar receptors (CR), INbiaxH, chaeMech	INsplitCR, MNcrab	2	celltype158	(Bezares-Calderón et al., 2018)
MNarm	Motoneuron, segments 1,2,3	INleucoPU	MUSac, MUSchae	6	celltype159	this study
INsnl	Head interneuron		INdecussPre	2	celltype160	this study
MNantacic	Motoneuron, segments 1,2		MUSob, MUSchae, MUSac	4	celltype161	this study
MNpostacic	Motoneuron, segments 1,2,3	INleucoPU	MUSob, MUSchae, MUSac	7	celltype162	this study
SN_DLSO1.3	Head sensory neuron, dorsolateral sense organ 1.3		SNPDF-dc	9	celltype163	this study
MNakro	Head ciliomotor neuron		akrotroch, metatroch,	2	celltype164	this study

			MNant			
MNche	Motoneuron, segments 1,2,3		MUSchae, MUSac	10	celltype165	this study
MNgland_head	Gland motoneuron, head	INDLSO, Ser-h1, INpreSer	ciliatedGland, MVGland, glia	2	celltype166	this study
SNstiff	Sensory neuron with stiff cilium, cryptic segment	SNPDF_pyg	INdesc, INPDF-lc	4	celltype167	this study
SNbronto	Sensory neuron, head		INsplitBronto, MC3cover, INrope	2	celltype168	this study
INcommascFV	Commissural ascending interneuron, FVaminde-positive, segment 2		INcommasc	3	celltype169	this study
SNpygM	Sensory neuron, pygidium		INasc_pyg, INsplit, SNPDF_pyg	2	celltype170	this study
INR1	Head interneuron	eyespotPRC_R1, adult eye PRC, INR1	SN_DLSO1.1, INR1, eyespotPRC_R1	4	celltype171	this study
SN_DLSO1.1	Head sensory neuron, dorsolateral sense organ	INR1, eyespot_PRC_R1, SN_LHSO2golden	-	2	celltype172	this study
SN_DLSO1.1_2/3	Head sensory neuron, dorsolateral sense organ	-	-	4	celltype173	this study
INmus	Head interneuron				celltype174	this study
INdescLuqinPDF	Head descending interneuron, PDF and luqin positive	SNPDF_pyg, INRGW, INpreSer	Ser-tr1, MNspinning	2	celltype175	this study
INcosplit	Trunk commissural pseudounipolar interneuron			2	celltype176	this study
INcommdescFVa	Trunk commissural descending interneuron, FVamide positive	SNFVa	MNladder, MNspinning	2	celltype177	this study
MNheadV	Head motoneuron	MNheadV	MUSlong, MNheadV	4	celltype178	this study
INsqNSasym	Head asymmetric interneuron	SNasym, INRGW, SNMIP	Ser-h1	1	celltype179	this study
INbiaxHmid	Trunk interneuron, segment 2		INasc_pyg	2	celltype180	this study

Table 1. Neuronal cell types in the *Platynereis* three-day-old larval connectome.

Cell types are listed in an order matching their CATMAID annotation (celltype1-180).

Neuronal morphological cell groups

Common name	description	Included cell types	# of cells	Catmaid annotation
INipsiasc	ipsilateral, ascending trunk interneurons	INATO_pyg, INasc_pyg, INFV_pyg	111	cellgroup1
INipsidesc	ipsilateral, descending trunk interneurons	INleucoPU	55	cellgroup2
INcommasc	commissural, ascending trunk interneurons	INcomm-Upstairs, INcomm-Upcross, INcommasc_FV, INpreLadder, INchaeMech	114	cellgroup3
INcommdesc	commissural, descending trunk interneurons	INcommdesc_FVa, INcomm-DownL	37	cellgroup4
INcomm	commissural trunk interneurons with no ascending or descending neurite	-	56	cellgroup5
INcosplit	commissural, pseudounipolar trunk interneurons	INcosplit_sg2	24	cellgroup6
INsplit	ipsilateral, pseudounipolar trunk interneurons	INCM, INsplitCR, INsplitCRATO, INsplitPB, INsplitPBant, INsplitPBant_RF/Ya, INsplitPUh, INsplitVent, INsplitBronto	114	cellgroup7
SN_LSO	lateral head sense organ sensory neurons	SN_NS18	27	cellgroup8
SNpyg	pygidial sensory neurons	Pygidial cirrus CR, PB and PU, SNPDF, SNpygM,	76	cellgroup9
SNpalp	palp immature sensory neurons	-	66	cellgroup10
SN_HSG3	immature sensory neurons of head sensory group 3	-	12	cellgroup11
INdecuss	decussating head interneurons	INdecussfoot, INdecusshook, INdecussPre, INW, INarc, INcrossbow, INpro	69	cellgroup12
INdesc	descending head interneurons	INrope, INbigloop, INMC3, INUturn, INdescLuqinPDF	33	cellgroup13
INbush	ventral head interneurons	-	6	cellgroup14

SNant, antCR, antPU	antennal sensory neurons, mostly immature	antCR, antPU	88	cellgroup15
SNcir	sensory neurons of cirri, mostly immature	-	60	cellgroup16
SNstomod	stomodeal sensory neurons, immature	-	51	cellgroup17
SNimmature_sg0	cryptic segment dorsal sensory organ, immature	-	15	cellgroup18

Table 2. Neuronal morphological cell groups in the *Platynereis* three-day-old larva.

Cell groups are listed in an order matching their CATMAID annotation (cellgroup1-18).

Non-neuronal cell types

Name	**description**	**Main presynaptic partners**	**# of cells**	**Catmaid annotation**	**reference**
akrotroch	akrotroch, with electron-dense filaments (annotation 'black fibers')	Loop, MNakro, MNant, Ser-tr1	8	celltype_non_neuronal1	(Verasztó et al., 2017a)
crescentcell	Crescent cell	Loop	1	celltype_non_neuronal2	(Verasztó et al., 2017a)
prototroch	prototroch	MC, Loop, MNant, cMNATO, Ser-h	23	celltype_non_neuronal3	(Verasztó et al., 2017a)
nuchal	Nuchal organ ciliated cells, with electron-dense filaments (annotation 'black fibers')	Loop	6	celltype_non_neuronal4	(Verasztó et al., 2017a)
metatroch	metatroch, with electron-dense filaments (annotation 'black fibers')	MNant, Ser-tr, MNakro	8	celltype_non_neuronal5	(Verasztó et al., 2017a)
paratroch	Paratroch, with electron-dense filaments (annotation 'black fibers')	Ser-tr, loop, MN, MNant, CiomRaphe	34	celltype_non_neuronal6	(Verasztó et al., 2017a)
spinGland	Major parapodial spinning gland	MNspinning	4	celltype_non_neuronal7	This study
covercell	Cover cell of prototroch, pigmented	cioMNcover, pygPBunp, MC3cover,	16	celltype_non_neuronal8	This study

		cATO, hPU2l_asymPDF			
ciliatedGland	Ciliated glands posterior to mouth	MNgland_head, (INdecusshook, INcrossbow, Ser.tr, MNant)	24	celltype_non_neuronal9	This study
eyespot_pigment_cell	Eyespot pigment cell	-	2	celltype_non_neuronal10	(Rhode, 1992)
pigment_cell_AE	Adult eye pigment cell	-	12	celltype_non_neuronal11	(Rhode, 1992)
Bright_droplets	Flattened cells containing bright droplets	-	10	celltype_non_neuronal12	This study
macrophage-like	macrophage-like cell with extended smooth ER	-	13	celltype_non_neuronal13	This study
Yolk cover cells	Cells with dark granules (probably lysosomes, diameter=0.82 µm, stdev=0.06, N=36) surrounding yolk	-	34	celltype_non_neuronal14	This study
Flat glia	Flattened glia with lots of RER	Ser-h, MN	19	celltype_non_neuronal15	This study
Radial-glia-like	Radial glia-like, without a cilium	MNax, MNgland	45	celltype_non_neuronal16	This study, similar to cells described by (Helm et al., 2017)
MVGland	Microvillar gland	MNgland	6	celltype_non_neuronal17	This study
microvillarCell	Cell with microvilli penetrating the cuticle	-	14	celltype_non_neuronal18	This study
protonephridium	protonephridium	-	4	celltype_non_neuronal19	This study
nephridium	metanephridium, with cilia	-	14	celltype_non_neuronal20	This study
nephridiumTip	nephridial tip, no cilia	-	2	celltype_non_neuronal21	This study
chaeta	chaeta	-	106	celltype_non_neuronal22	Jasek et al.
acicula	acicula	-	12	celltype_non_neuronal23	Jasek et al.
circumacicular	Cells around acicula	-	54	celltype_non_neuronal24	Jasek et al.
hemichaetal	Cells with villi forming a semi-circle around the most proximal part of chaeta	-	175	celltype_non_neuronal25	Jasek et al., follicle cells described in (Tilic and Bartolomaeus, 2016)

ER_circumchaetal	Forms full circle around proximal part of chaeta, with villi and characteristic RER lumen	-	46	celltype_non_neuronal26	Jasek et al., follicle cells described in (Tilic and Bartolomaeus, 2016)
noER_circumchaetal	Encircles mid part of chaeta, with no villi and very little ER	-	94	celltype_non_neuronal27	Jasek et al.
EC_circumchaetal	Epithelial cells encircling distal part of chaeta	-	106	celltype_non_neuronal28	Jasek et al.
HeadGland	Anterior head glands	-	5	celltype_non_neuronal29	This study
InterparaGland	Interparapodial gland	SNVNC	4	celltype_non_neuronal30	This study
spinMicroGland	Small spinning gland	-	19	celltype_non_neuronal31	This study
EC	Epithelial cell		974	celltype_non_neuronal32	This study
vacuolar_cell_head	EC with bright pigment vacuoles between head glands	pygPBup	3	celltype_non_neuronal33	This study
Glia pigmented	Pigmented glia	sporadic	5	celltype_non_neuronal34	This study
pygidial_pigment_cell	Pygidial pigment cell	INsplitCRATO, loop, pygPBunp, INsplitPB	26	celltype_non_neuronal35	This study
Blanket cell	Flattened cells lining organs	-	75	celltype_non_neuronal36	This study
MUSac_notA	anterior notopodial acicular muscle	MNring; MNcrab; MNwave; MNantacic	12	celltype_non_neuronal37	Jasek et al.
MUSac_notP	posterior notopodial acicular muscle	MNacic; MNwave; MNbow; MNspider; MNcrab;	12	celltype_non_neuronal38	Jasek et al.
MUSac_notM	middle notopodial acicular muscle	MNwave	12	celltype_non_neuronal39	Jasek et al.
MUSac_neuAV	anterior ventral neuropodial acicular muscle	MNcrab	16	celltype_non_neuronal40	Jasek et al.
MUSac_neuPD	posterior dorsal neuropodial acicular muscle	sparse	18	celltype_non_neuronal41	Jasek et al.
MUSac_neuPV	posterior ventral neuropodial	MNcrab; MNspider;	14	celltype_non_neuronal42	Jasek et al.

	acicular muscle	MNslide; MNring; MNperifac			
MUSac_neuDy	neuropodial Y	sparse	4	celltype_non_neuronal43	Jasek et al.
MUSac_neuDx	dorsal neuropodial muscle to notopodium	Weak MN crab	8	celltype_non_neuronal44	Jasek et al.
MUSac_neuDach	dorsal neuropodial chaetal muscle	MNarm, MNac	18	celltype_non_neuronal45	Jasek et al.
MUSac_neure	Chaetal sac retractor	-	8	celltype_non_neuronal46	Jasek et al.
MUSac_i	Interacicular muscle	-	6	celltype_non_neuronal47	Jasek et al.
MUSob-ant_re	parapodial retractor muscle	MNspider; MNantacic; MNhose; MNob-contra	39	celltype_non_neuronal48	Jasek et al.
MUSob-ant_arc	ventral parapodial muscle arc	MNspider; MNantacic	18	celltype_non_neuronal49	Jasek et al.
MUSob-ant_m-pp	medial oblique to mid-parapodiuml	MNob-contra; MNhose; MNcrab	12	celltype_non_neuronal50	Jasek et al.
MUSob-ant_ml-pp	Mediolateral oblique to mid-parapodium	MNhose; MNob-contra	4	celltype_non_neuronal51	Jasek et al.
MUSob-ant_l-pp	lateral oblique to mid-parapodium	MNob-contra; MNhose; MNring; MN_oblique; MNspider	10	celltype_non_neuronal52	Jasek et al.
MUSob-ant_trans	oblique to start of transverse	MNhose	10	celltype_non_neuronal53	Jasek et al.
MUSob-post_notD	notopodial dorsal oblique muscle	MNpostacic	28	celltype_non_neuronal54	Jasek et al.
MUSob-post_neuDlong	neuropodial dorsal oblique long	MNspider; MNpostacic; MNring	9	celltype_non_neuronal55	Jasek et al.
MUSob-post_neuDprox	neuropodial dorsal oblique proximal	MNspider	18	celltype_non_neuronal56	Jasek et al.
MUSob-post_neuDdist	neuropodial dorsal oblique distal	MNbow	19	celltype_non_neuronal57	Jasek et al.
MUSob-post_neuV	posterior ventral neuropodial muscle	MNspider; MNhose; MNob-ipsi; MN_oblique; MNring;	38	celltype_non_neuronal58	Jasek et al.
MUSob-post_notV	posterior ventral notopodial muscle	MNhose; MNspider; MNhose; MNob-	18	celltype_non_neuronal59	Jasek et al.

		ipsi; MN_oblique			
MUSob-postM	oblique to distal interacicular	-	4	celltype_non_neuronal60	Jasek et al.
MUSob-post_noty	oblique to body wall near distal interacicular and neuropodial Y	MNhose; MNob-ipsi; MNspider;	6	celltype_non_neuronal61	Jasek et al.
MUSob-post_i	distal interacicular muscle	-	6	celltype_non_neuronal62	Jasek et al.
MUSchae_notDob	notochaetal next to dorsal oblique	MNpostacic;	18	celltype_non_neuronal63	Jasek et al.
MUSchae_notD	dorsal notopodial chaetal sac muscle	MNpostacic	6	celltype_non_neuronal64	Jasek et al.
MUSchae_notDn	next to dorsal notopodial chaetal sac muscle	-	6	celltype_non_neuronal65	Jasek et al.
MUSchae_notA	anterior notopodial chaetal sac muscle	MNspider; MNantacic	6	celltype_non_neuronal66	Jasek et al.
MUSchae_notAac	notopodial chaetal muscle under acicula	MNcrab; MNbiramous; MNwave; MNantacic; MNacic;	24	celltype_non_neuronal67	Jasek et al.
MUSchae_notAre	notopodial retractor muscle	-	4	celltype_non_neuronal68	Jasek et al.
MUSchae_neuVob	neurochaetal next to ventral oblique	MNche	16	celltype_non_neuronal69	Jasek et al.
MUSchae_neuDac	neuropodial chaetal muscle under acicula	MNbiramous; MNche; MNspider	28	celltype_non_neuronal70	Jasek et al.
MUSchae_neuAVo	anterior ventral neurochaetal muscle ob	MNarm; MNche	16	celltype_non_neuronal71	Jasek et al.
MUSchae_neuAVt	anterior ventral neurochaetal muscle trans	MNspider; MNslide	6	celltype_non_neuronal72	Jasek et al.
MUSchae_Are	chaetal sac under parapodial retractor	MNbiramous; MNspider	6	celltype_non_neuronal73	Jasek et al.
MUStrans	transverse muscle	MNring; MNhose; MNsmile; MNob-contra; MNladder	62	celltype_non_neuronal74	Jasek et al.
MUSlong_D	Dorsolateral muscle	MNring; MN; MNcrab	86	celltype_non_neuronal75	Jasek et al.
MUSlong_V	ventrolateral muscle	MN; MNring; MNcrab; MNsmile; MNspider	82	celltype_non_neuronal76	Jasek et al.

MUSax	axochord	MNax; MNcomm	12	celltype_non_neuronal77	Jasek et al.
MUS_pygidium_ring	Pygidial ring muscle	-	1	celltype_non_neuronal78	Jasek et al.
MUSph	Pharyngeal muscle	-	50	celltype_non_neuronal79	Jasek et al.
MUSll	Lower lip muscle	MNsmile	10	celltype_non_neuronal80	Jasek et al.
MUSant	antenna muscle	-	8	celltype_non_neuronal81	Jasek et al.
MUSly	Lyrate muscle	-	6	celltype_non_neuronal82	Jasek et al.
MUSpl	palp muscle	-	4	celltype_non_neuronal83	Jasek et al.
MUSci	Cirrus muscle	-	4	celltype_non_neuronal84	Jasek et al.
MUSch	Cheek muscle	MNsmile	6	celltype_non_neuronal85	Jasek et al.
MUSpx	Plexus muscle	-	1	celltype_non_neuronal86	Jasek et al.
MUSpr-vt	ventral transverse muscle of prostomium	-	1	celltype_non_neuronal87	Jasek et al.
MUStri	Triangle muscle	-	2	celltype_non_neuronal88	Jasek et al.
MUSmed_head	smooth head muscles	-	2	celltype_non_neuronal89	Jasek et al.
CB_pigment	Ciliary band pigment cell	MC3cover (sporadic)	58	celltype_non_neuronal90	This study

Table 3. Non-neuronal cell types in the *Platynereis* three-day-old larva.

Cell types are listed in an order matching their CATMAID annotation (celltype_non_neuronal1-89).

Catmaid projects	**Number of layers imaged (z)**	**Layer dimensions (x,y) in pixels**	**Resolution (x,y,z) nm/pixels**
HT-4_Naomi_project	4845	25792, 28800	5.7, 5.7, 40
Plexus_HT-4_Naomi_project__372-4013	1407	43920, 40968	2.2, 2.2, 40

Immuno_HT-4_Naomi_project	13	50000, 52000	2.2, 2.2, 40
Jump_864_HT-4_Naomi_project__853-873	21	60000, 60000	2.2, 2.2, 40
Jump_2800_HT-4_Naomi_project__2762-2818	57	44702, 26371	2.2, 2.2, 40
Jump_3725_HT-4_Naomi_project__3719-3728	10	24000, 26000	3.7, 3.7, 40

Table 4. CATMAID accessory project layers related to the main HT9-4 (NAOMI) stack.
Summary of the extra project stacks that were created by re-imaging the main data set at higher resolutions. This was needed to resolve some inconsistencies and hard-to-trace layers.

References

Achim K, Pettit J-B, Saraiva LR, Gavriouchkina D, Larsson T, Arendt D, Marioni JC. 2015. High-throughput spatial mapping of single-cell RNA-seq data to tissue of origin. *Nat Biotechnol* **33**:503–509.

Arendt D. 2008. The evolution of cell types in animals: emerging principles from molecular studies. *Nature Reviews Genetics*. doi:10.1038/nrg2416

Asadulina A, Panzera A, Verasztó C, Liebig C, Jékely G. 2012. Whole-body gene expression pattern registration in Platynereis larvae. *Evodevo* **3**:27.

Ayers T, Tsukamoto H, Gühmann M, Veedin Rajan VB, Tessmar-Raible K. 2018. A G-type opsin mediates the shadow reflex in the annelid Platynereis dumerilii. *BMC Biol* **16**:41.

Bates AS, Manton JD, Jagannathan SR, Costa M, Schlegel P, Rohlfing T, Jefferis GS. 2020. The natverse, a versatile toolbox for combining and analysing neuroanatomical data. *Elife* **9**. doi:10.7554/eLife.53350

Bentley B, Branicky R, Barnes CL, Chew YL, Yemini E, Bullmore ET, Vértes PE, Schafer WR. 2016. The Multilayer Connectome of Caenorhabditis elegans. *PLoS Comput Biol* **12**:e1005283.

Bezares-Calderón LA, Berger J, Jasek S, Verasztó C, Mendes S, Gühmann M, Almeda R, Shahidi R, Jékely G. 2018. Neural circuitry of a polycystin-mediated hydrodynamic startle response for predator avoidance. *eLife*. doi:10.7554/elife.36262

Brunet T, Fischer AH, Steinmetz PR, Lauri A, Bertucci P, Arendt D. 2016. The evolutionary origin of bilaterian smooth and striated myocytes. *Elife* **5**. doi:10.7554/eLife.19607

Cao C, Lemaire LA, Wang W, Yoon PH, Choi YA, Parsons LR, Matese JC, Levine M, Chen K. 2019. Comprehensive single-cell transcriptome lineages of a proto-vertebrate. *Nature* **571**:349–354.

Cardona A, Saalfeld S, Schindelin J, Arganda-Carreras I, Preibisch S, Longair M, Tomancak P, Hartenstein V, Douglas RJ. 2012. TrakEM2 software for neural circuit reconstruction. *PLoS One* **7**:e38011.

Carreira-Rosario A, Zarin AA, Clark MQ, Manning L, Fetter RD, Cardona A, Doe CQ. 2018. MDN brain descending neurons coordinately activate backward and inhibit forward locomotion. *Elife* **7**. doi:10.7554/eLife.38554

Chartier TF, Deschamps J, Dürichen W, Jékely G, Arendt D. 2018. Whole-head recording of chemosensory activity in the marine annelid. *Open Biol* **8**. doi:10.1098/rsob.180139

Conzelmann M, Williams EA, Tunaru S, Randel N, Shahidi R, Asadulina A, Berger J, Offermanns S, Jékely G. 2013. Conserved MIP receptor-ligand pair regulates Platynereis larval settlement. *Proc Natl Acad Sci U S A* **110**:8224–8229.

Cook SJ, Jarrell TA, Brittin CA, Wang Y, Bloniarz AE, Yakovlev MA, Nguyen KCQ, Tang LT-H, Bayer EA, Duerr JS, Bülow HE, Hobert O, Hall DH, Emmons SW. 2019. Whole-animal connectomes of both Caenorhabditis elegans sexes. *Nature* **571**:63–71.

Costa M, Manton JD, Ostrovsky AD, Prohaska S, Gregory S X. 2016. NBLAST: Rapid, Sensitive

Comparison of Neuronal Structure and Construction of Neuron Family Databases. *Neuron*. doi:10.1016/j.neuron.2016.06.012

Deng B, Li Q, Liu X, Cao Y, Li B, Qian Y, Xu R, Mao R, Zhou E, Zhang W, Huang J, Rao Y. 2019. Chemoconnectomics: Mapping Chemical Transmission in Drosophila. *Neuron* **101**:876–893.e4.

Dorsett DA. 1964. The sensory and motor innervation of Nereis. *Proc R Soc Lond B Biol Sci* **159**:652–667.

Eckstein N, Bates AS, Du M, Hartenstein V, Gregory S X, Funke J. 2020 Neurotransmitter Classification from Electron Microscopy Images at Synaptic Sites in Drosophila. doi:10.1101/2020.06.12.148775

Fischer AH, Henrich T, Arendt D. 2010. The normal development of Platynereis dumerilii (Nereididae, Annelida). *Front Zool* **7**:31.

Hausen H. 2005. Comparative structure of the epidermis in polychaetes (Annelida). *Hydrobiologia*. doi:10.1007/s10750-004-4442-x

He L, Gulyanon S, Mihovilovic Skanata M, Karagyozov D, Heckscher ES, Krieg M, Tsechpenakis G, Gershow M, Tracey WD Jr. 2019. Direction Selectivity in Drosophila Proprioceptors Requires the Mechanosensory Channel Tmc. *Curr Biol* **29**:945–956.e3.

Helm C, Karl A, Beckers P, Kaul-Strehlow S, Ulbricht E, Kourtesis I, Kuhrt H, Hausen H, Bartolomaeus T, Reichenbach A, Bleidorn C. 2017. Early evolution of radial glial cells in Bilateria. *Proc Biol Sci* **284**. doi:10.1098/rspb.2017.0743

Helmstaedter M. 2013. Cellular-resolution connectomics: challenges of dense neural circuit reconstruction. *Nat Methods* **10**:501–507.

Hobert O, Glenwinkel L, White J. 2016. Revisiting Neuronal Cell Type Classification in Caenorhabditis elegans. *Curr Biol* **26**:R1197–R1203.

Horridge GA. 1963. Proprioceptors, bristle receptors, efferent sensory impulses, neurofibrils and number of axons in the parapodial nerve of the polychaete Harmothoë. *Proceedings of the Royal Society of London Series B Biological Sciences* **157**:199–222.

Jékely G, Colombelli J, Hausen H, Guy K, Stelzer E, Nédélec F, Arendt D. 2008. Mechanism of phototaxis in marine zooplankton. *Nature* **456**:395–399.

Kebschull JM, Ringach N, Richman EB, Friedmann D, Kolluru SS, Jones RC, Allen WE, Wang Y, Zhou H, Cho SW, Chang H, Deisseroth K, Quake SR, Luo L. 2020 Cerebellar nuclei evolved by repeatedly duplicating a conserved cell type set. doi:10.1101/2020.06.25.170118

Miroschnikow A, Schlegel P, Schoofs A, Hueckesfeld S, Li F, Schneider-Mizell CM, Fetter RD, Truman JW, Cardona A, Pankratz MJ. 2018. Convergence of monosynaptic and polysynaptic sensory paths onto common motor outputs in a Drosophila feeding connectome. *eLife*. doi:10.7554/elife.40247

Morgan JL, Lichtman JW. 2013. Why not connectomics? *Nature Methods*. doi:10.1038/nmeth.2480

Nielsen C, Brunet T, Arendt D. 2018. Evolution of the bilaterian mouth and anus. *Nat Ecol Evol* **2**:1358–1376.

Ohyama T, Schneider-Mizell CM, Fetter RD, Aleman JV, Franconville R, Rivera-Alba M, Mensh BD, Branson KM, Simpson JH, Truman JW, Cardona A, Zlatic M. 2015. A multilevel multimodal circuit enhances action selection in Drosophila. *Nature* **520**:633–639.

Puhl JG, Masino MA, Mesce KA. 2012. Necessary, sufficient and permissive: a single locomotor command neuron important for intersegmental coordination. *J Neurosci* **32**:17646–17657.

Randel N, Asadulina A, Bezares-Calderón LA, Verasztó C, Williams EA, Conzelmann M, Shahidi R, Jékely G. 2014. Neuronal connectome of a sensory-motor circuit for visual navigation. *Elife* **3**. doi:10.7554/eLife.02730

Randel N, Bezares-Calderón LA, Gühmann M, Shahidi R, Jékely G. 2013. Expression dynamics and protein localization of rhabdomeric opsins in Platynereis larvae. *Integr Comp Biol* **53**:7–16.

Randel N, Shahidi R, Verasztó C, Bezares-Calderón LA, Schmidt S, Jékely G. 2015. Inter-individual stereotypy of the Platynereis larval visual connectome. *Elife* **4**:e08069.

Rhode B. 1992. Development and differentiation of the eye in Platynereis dumerilii (Annelida, Polychaeta). *J Morphol* **212**:71–85.

Ryan K, Lu Z, Meinertzhagen IA. 2016. The CNS connectome of a tadpole larva of Ciona intestinalis (L.) highlights sidedness in the brain of a chordate sibling. *eLife*. doi:10.7554/elife.16962

Saalfeld S, Cardona A, Hartenstein V, Tomancak P. 2009. CATMAID: collaborative annotation toolkit for massive amounts of image data. *Bioinformatics* **25**:1984–1986.

Schlegel P, Costa M, Jefferis GS. 2017. Learning from connectomics on the fly. *Curr Opin Insect Sci*

24:96–105.
Schlegel P, Texada MJ, Miroschnikow A, Schoofs A, Hückesfeld S, Peters M, Schneider-Mizell CM, Lacin H, Li F, Fetter RD, Truman JW, Cardona A, Pankratz MJ. 2016. Synaptic transmission parallels neuromodulation in a central food-intake circuit. *Elife* **5**. doi:10.7554/eLife.16799
Schneider-Mizell CM, Gerhard S, Longair M, Kazimiers T, Li F, Zwart MF, Champion A, Midgley FM, Fetter RD, Saalfeld S, Cardona A. 2016. Quantitative neuroanatomy for connectomics in Drosophila. *Elife* **5**. doi:10.7554/eLife.12059
Schorb M, Haberbosch I, Hagen WJH, Schwab Y, Mastronarde DN. 2019. Software tools for automated transmission electron microscopy. *Nat Methods* **16**:471–477.
Sedgwick A. 1884. On the origin of metameric segmentation and some other morphological questions. *Q J Microsc Sci* **24**:43–82.
Shahidi R, Williams EA, Conzelmann M, Asadulina A, Verasztó C, Jasek S, Bezares-Calderón LA, Jékely G. 2015. A serial multiplex immunogold labeling method for identifying peptidergic neurons in connectomes. *Elife* **4**. doi:10.7554/eLife.11147
Sholl DA. 1953. Dendritic organization in the neurons of the visual and motor cortices of the cat. *J Anat* **87**:387–406.
Singla CL. 1975. Statocysts of hydromedusae. *Cell and Tissue Research*. doi:10.1007/bf00223835
Starunov VV, Dray N, Belikova EV, Kerner P, Vervoort M, Balavoine G. 2015. A metameric origin for the annelid pygidium? *BMC Evol Biol* **15**:25.
Steinmetz PRH, Kostyuchenko RP, Fischer A, Arendt D. 2011. The segmental pattern of otx, gbx, and Hox genes in the annelid Platynereis dumerilii. *Evol Dev* **13**:72–79.
Tilic E, Bartolomaeus T. 2016. Structure, function and cell dynamics during chaetogenesis of abdominal uncini in Sabellaria alveolata (Sabellariidae, Annelida). *Zoological Lett* **2**:1.
Tomer R, Denes AS, Tessmar-Raible K, Arendt D. 2010. Profiling by image registration reveals common origin of annelid mushroom bodies and vertebrate pallium. *Cell* **142**:800–809.
Tosches MA. 2017. Developmental and genetic mechanisms of neural circuit evolution. *Dev Biol* **431**:16–25.
Vaadia RD, Li W, Voleti V, Singhania A, Hillman EMC, Grueber WB. 2019. Characterization of Proprioceptive System Dynamics in Behaving Drosophila Larvae Using High-Speed Volumetric Microscopy. *Curr Biol* **29**:935–944.e4.
Verasztó C, Gühmann M, Jia H, Rajan VBV, Bezares-Calderón LA, Piñeiro-Lopez C, Randel N, Shahidi R, Michiels NK, Yokoyama S, Tessmar-Raible K, Jékely G. 2018. Ciliary and rhabdomeric photoreceptor-cell circuits form a spectral depth gauge in marine zooplankton. *Elife* **7**. doi:10.7554/eLife.36440
Verasztó C, Ueda N, Bezares-Calderón LA, Panzera A, Williams EA, Shahidi R, Jékely G. 2017a. Ciliomotor circuitry underlying whole-body coordination of ciliary activity in the larva. *Elife* **6**. doi:10.7554/eLife.26000
Verasztó C, Ueda N, Bezares-Calderón LA, Panzera A, Williams EA, Shahidi R, Jékely G. 2017b. Ciliomotor circuitry underlying whole-body coordination of ciliary activity in the Platynereis larva. *eLife*. doi:10.7554/elife.26000
Vergara HM, Bertucci PY, Hantz P, Tosches MA, Achim K, Vopalensky P, Arendt D. 2017. Whole-organism cellular gene-expression atlas reveals conserved cell types in the ventral nerve cord of Platynereis dumerilii. *Proceedings of the National Academy of Sciences*. doi:10.1073/pnas.1610602114
Vergara HM, Pape C, Meechan K, Zinchenko V, Genoud C, Wanner AA, Titze B, Templin R, Bertucci PY, Simakov O, Machado P, Savage EL, Schwab Y, Friedrich RW, Kreshuk A, Tischer C, Arendt D. 2020 Whole-body integration of gene expression and single-cell morphology. doi:10.1101/2020.02.26.961037
White JG, Southgate E, Thomson JN, Brenner S. 1986. The structure of the nervous system of the nematode Caenorhabditis elegans. *Philos Trans R Soc Lond B Biol Sci* **314**:1–340.
Williams EA, Conzelmann M, Jékely G. 2015. Myoinhibitory peptide regulates feeding in the marine annelid Platynereis. *Front Zool* **12**:1.
Williams EA, Jékely G. 2019. Neuronal cell types in the annelid Platynereis dumerilii. *Curr Opin Neurobiol* **56**:106–116.
Williams EA, Verasztó C, Jasek S, Conzelmann M, Shahidi R, Bauknecht P, Mirabeau O, Jékely G. 2017. Synaptic and peptidergic connectome of a neurosecretory center in the annelid brain. *Elife* **6**. doi:10.7554/eLife.26349
Zarin AA, Mark B, Cardona A, Litwin-Kumar A, Doe CQ. 2019 ADrosophilalarval premotor/motor

neuron connectome generating two behaviors via distinct spatio-temporal muscle activity. doi:10.1101/617977

Zheng Z, Lauritzen JS, Perlman E, Robinson CG, Nichols M, Milkie D, Torrens O, Price J, Fisher CB, Sharifi N, Calle-Schuler SA, Kmecova L, Ali IJ, Karsh B, Trautman ET, Bogovic JA, Hanslovsky P, Jefferis GSXE, Kazhdan M, Khairy K, Saalfeld S, Fetter RD, Bock DD. 2018. A Complete Electron Microscopy Volume of the Brain of Adult Drosophila melanogaster. *Cell* **174**:730–743.e22.

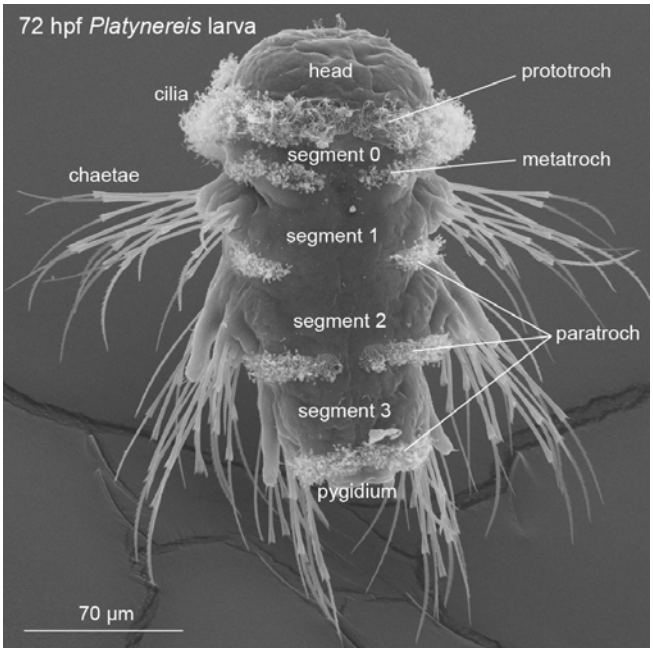

Figure 1 – figure supplement 1. Anatomy of the three-day-old *Platynereis* larva.
Scanning EM image of a three-day-old *Platynereis* larva (72 hours post fertilisation) with the main body regions labelled.

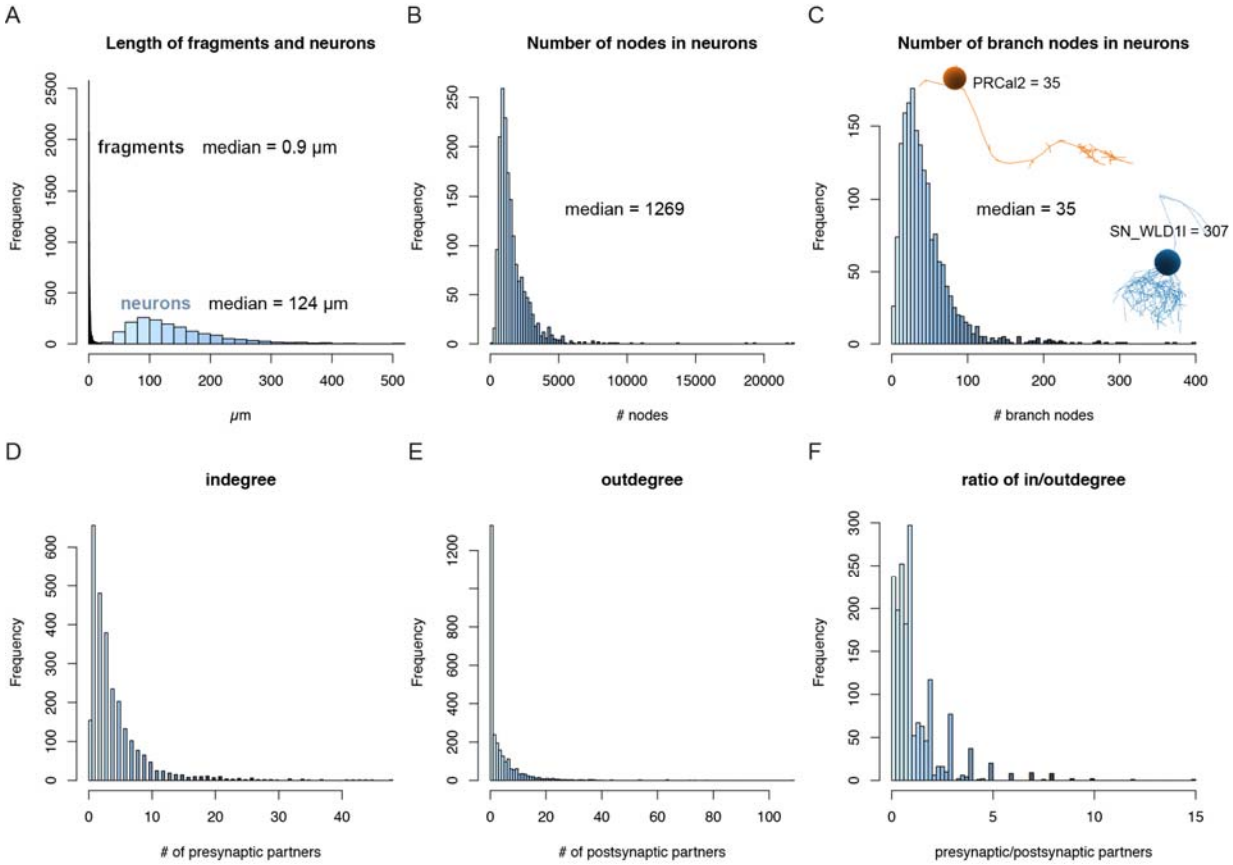

Figure 1 – figure supplement 2. Skeleton statistics of the *Platynereis* larval connectome.
(A) Length distribution of fragments and neurons with soma in the connectome set. (B) Histogram of the number of nodes in connectome neurons. (C) Histogram of the number of branch nodes in the connectome neurons. The images show example neurons with a simple (PRCal2) and a highly branched skeleton (SN_WLD1l). (D) Indigree distribution of all cells in the connectome set. (E) Outdegree distribution of all cells in the connectome set. (F) The distribution of the ratio of indegree to outdegree for all cells in the connectome set.

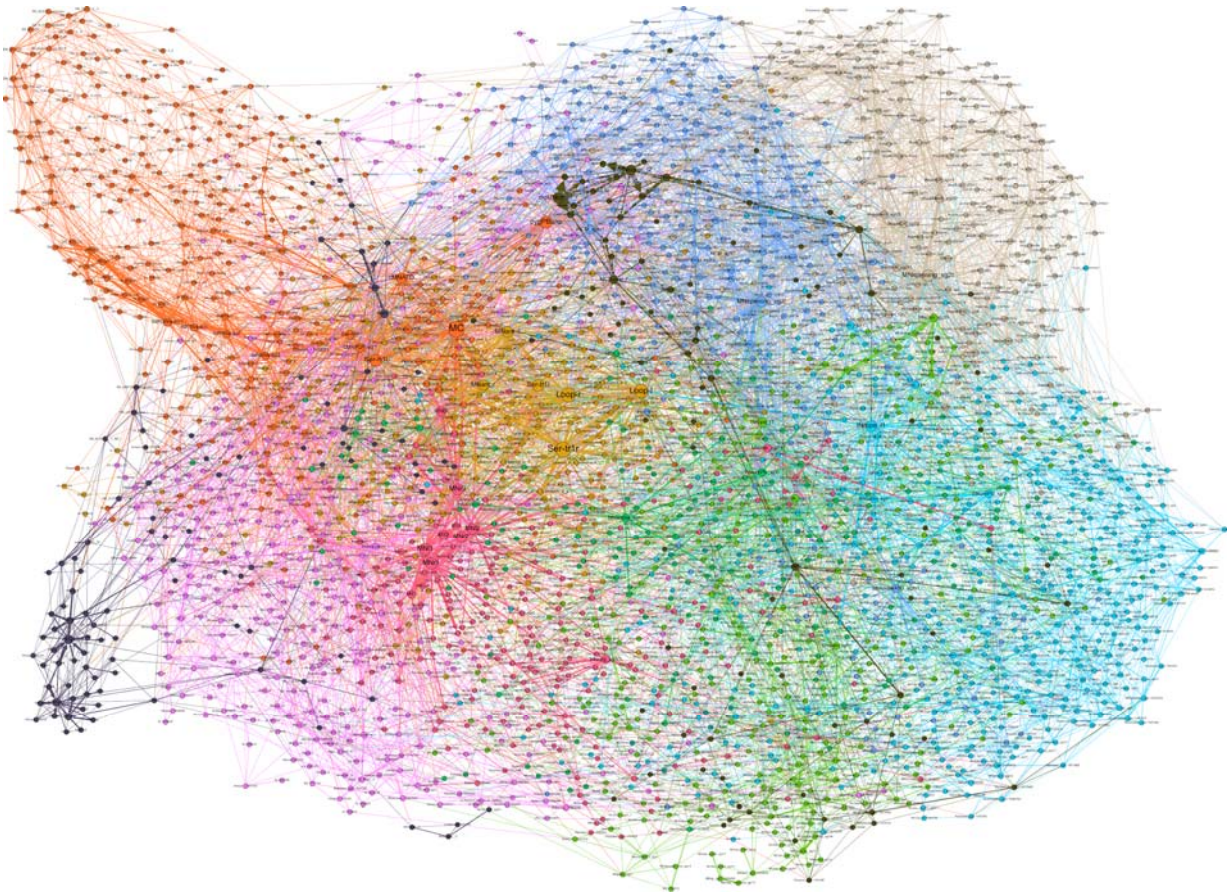

Figure 1 – figure supplement 3. The *Platynereis* larval connectome with node labels.
Graph representation of the connectome with nodes representing single cells and edges synaptic connectivity. The graph includes 2,728 nodes and 11,403 edges.

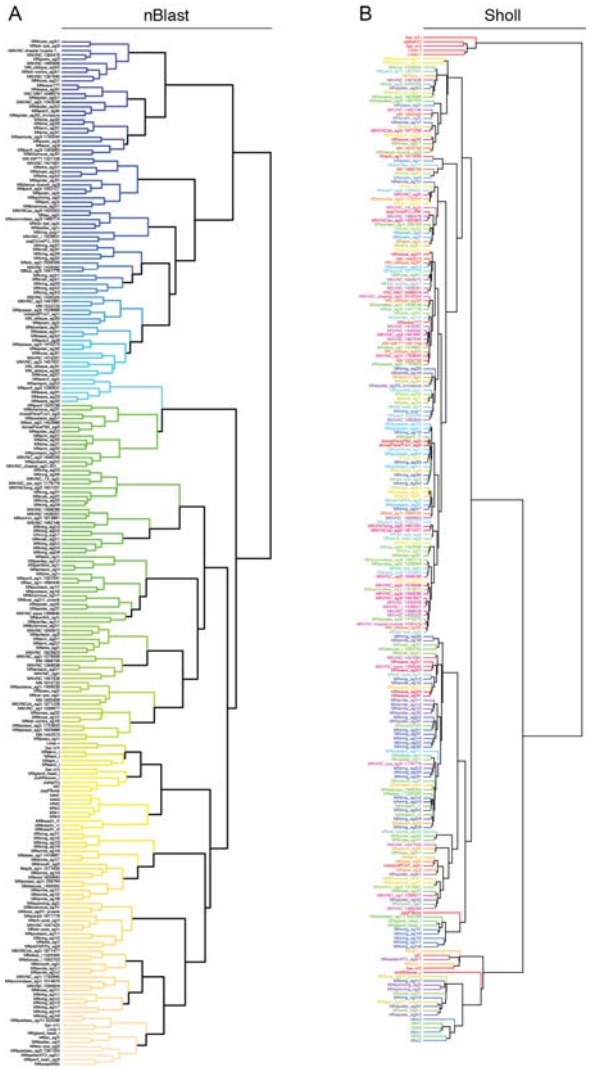

Figure 3 – figure supplement 1. Clustering of motoneurons based on NBlast and Sholl analysis.
(A) Dendrogram of 237 motoneurons based on NBLAST scores. (B) Dendrogram of 237 motoneurons based on Sholl analysis scores. In B neurons that we defined as cell types have similar colours.

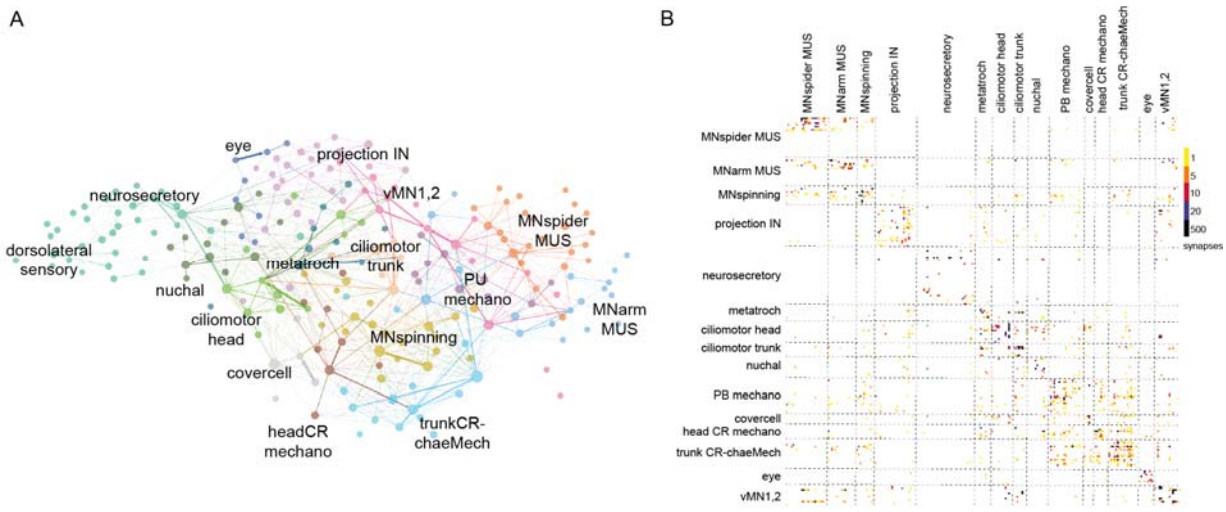

Figure 3 – figure supplement 2. Modules in the cell-type connectome.
(A) Modules in the cell-type connectome. (B) Connectivity matrix of the graph in Figure 3, dashed lines delineate the modules coloured in A.

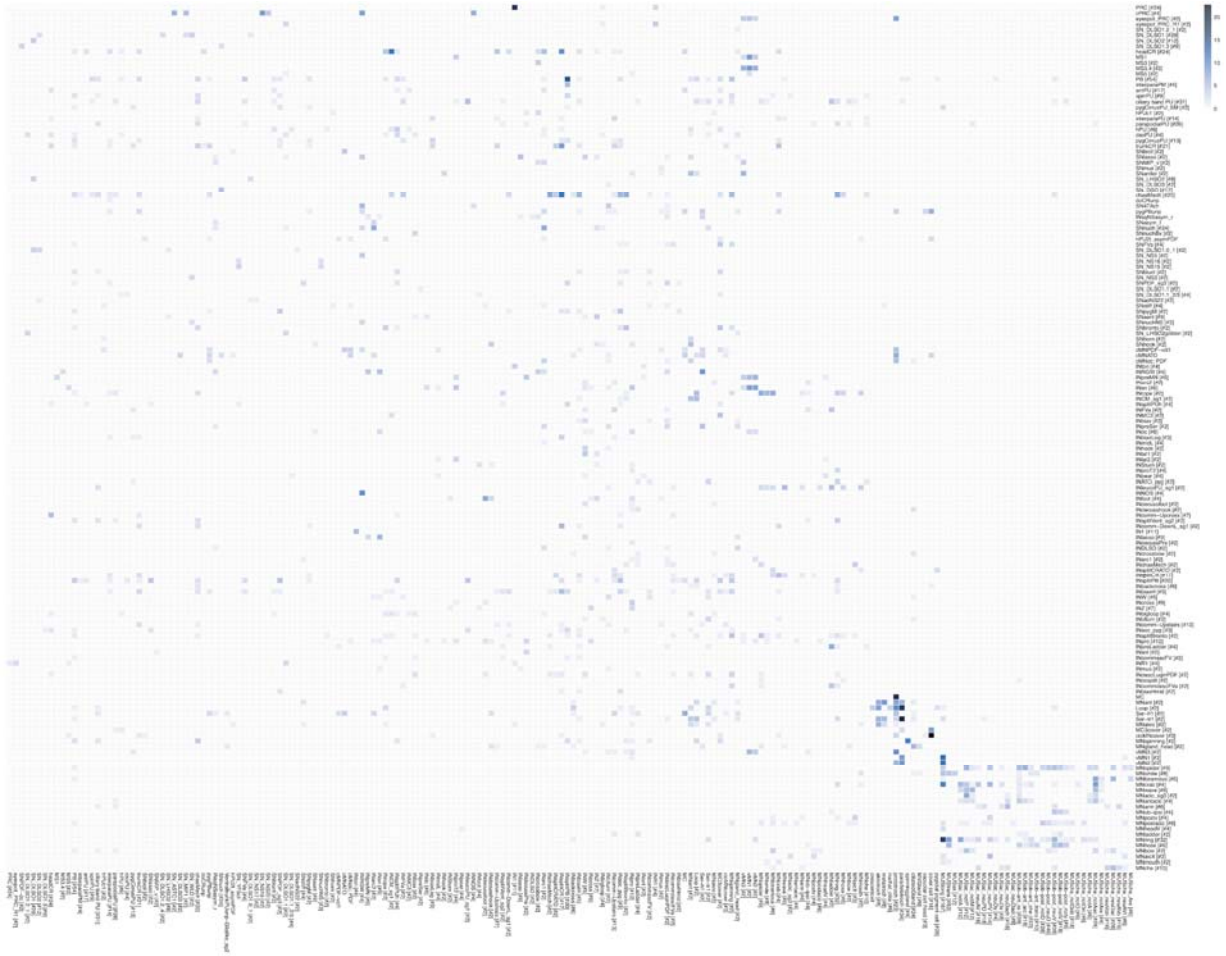

Figure 3 – figure supplement 3. Connectivity matrix of the cell-type connectome.

Grouped connectivity matrix of cell types. The number of cells of the same type in a group is shown in square brackets. The scale represents the square root of the number of synapses. Presynaptic groups are shown on the right side.

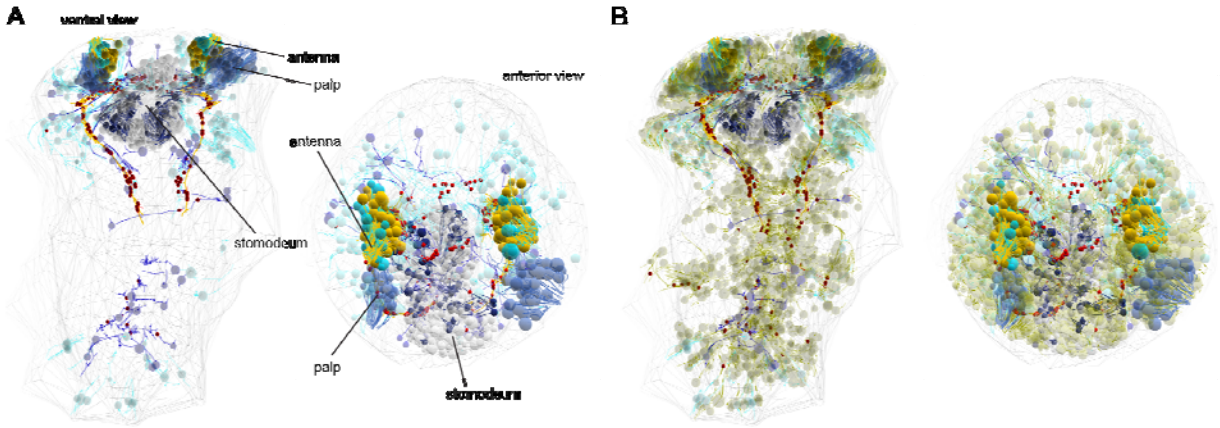

Figure 3 – figure supplement 4. Developing sensory neurons.
(A) Reconstruction of antennal, palp and stomodeal cells. The cyan cells in the antennal group are differentiated. All other cells are immature, with immature sensory dendrites and few synapses. Ventral and anterior views. Presynaptic sites are shown as red dots. (B) The same cells shown together with 1,692 non-differentiated cells that putatively belong to the neuronal lineage.

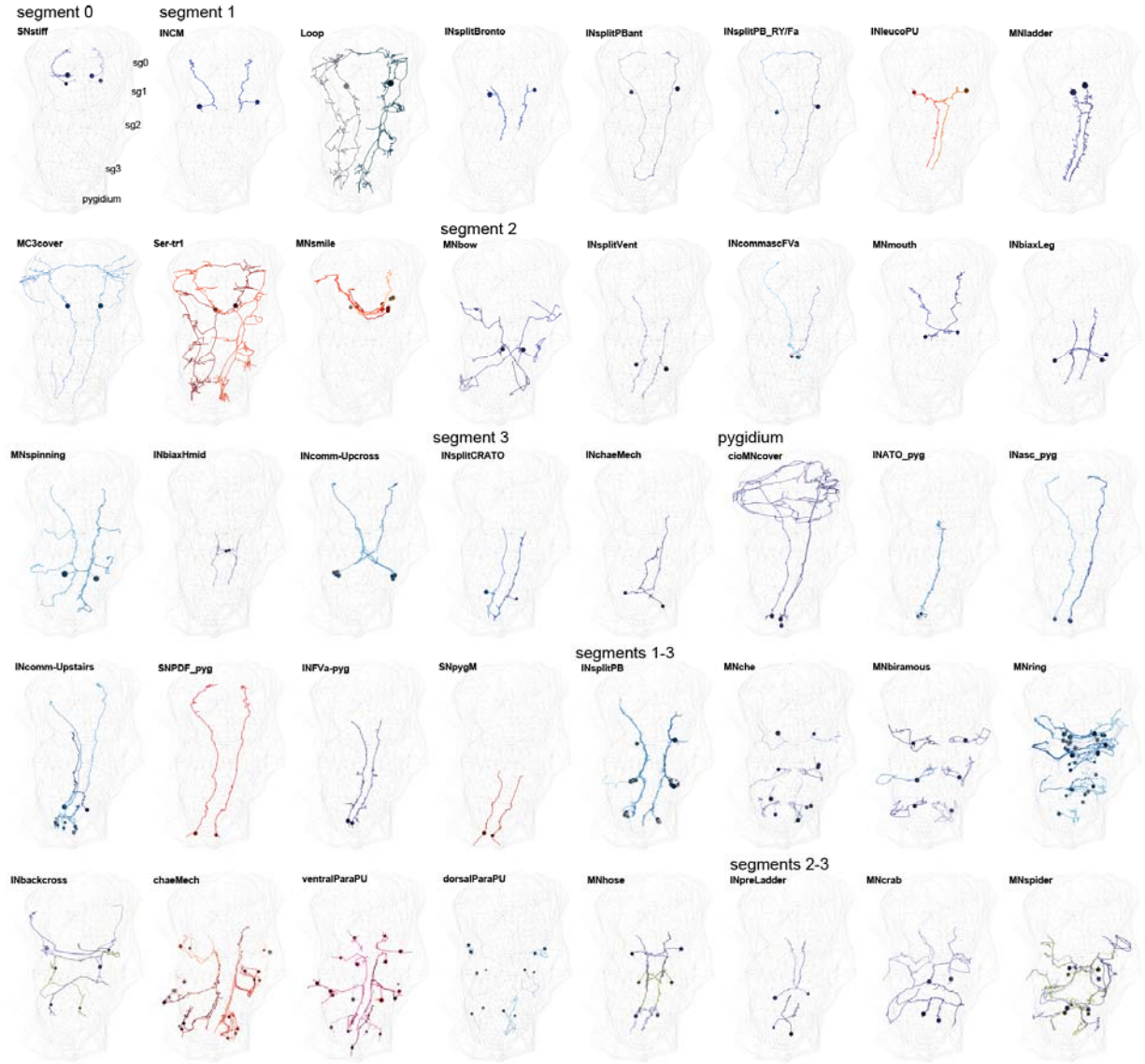

Figure 7 – figure supplement 1. Segment-specific and segmentally iterated cell types.
EM reconstructions of sensory, inter- and motor neuron types present in different combinations of trunk segments.

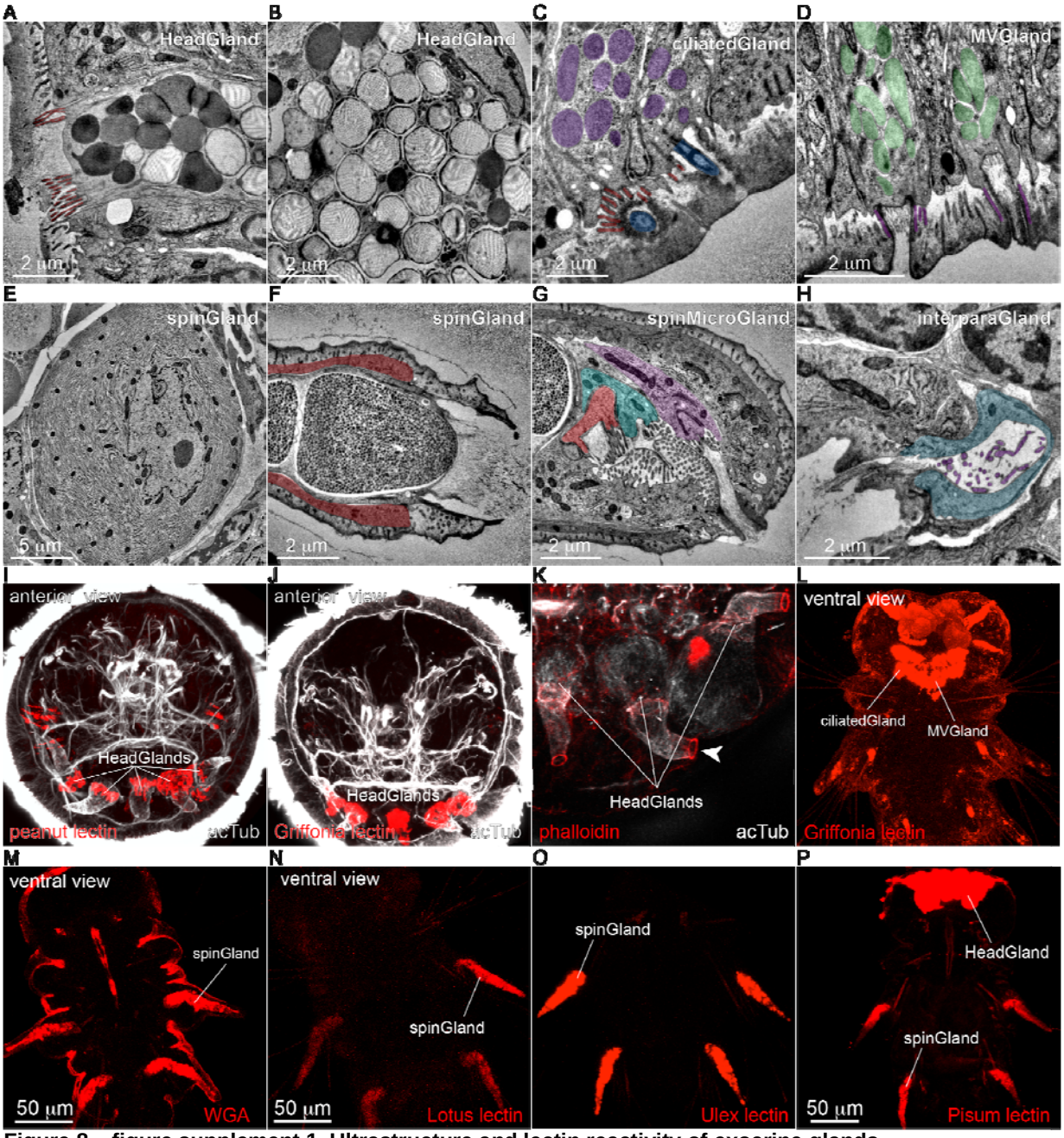

Figure 8 – figure supplement 1. Ultrastructure and lectin reactivity of exocrine glands.
(A) TEM image of the secretory pore of a head gland cell. (B) Secretory vesicles in a head gland cell. (C) TEM image of a ciliated gland cell. The cilium, microvilli and vesicles are highlighted. (D) A microvillar gland cell. The microvilli and vesicles are highlighted. (E) Soma of a spinning gland cell with the extended ER. (F) Secretory pore of a spinning gland cell. (G) Secretory pore of three spin micro gland cells adjacent to the pore of the spinning gland cell. (H) Secretory pore of an interparapodial gland cell. (I) Staining of headGland cells with peanut lectin in a two-day-old larva, anterior view. (J) Staining of headGland cells with Griffonia lectin in a two-day-old larva, anterior view. (K) Phalloidin staining of the secretory pore of head gland cells. (L) Staining of ciliateGland and MVGland cells with Griffonia lectin in a three-day-old larva, ventral view. (M) Staining of spinGland cells with wheat germ agglutinin in a three-day-old larva, ventral view. (N) Staining of spinGland cells with Lotus lectin in a three-day-old larva, ventral view. (O) Staining of spinGland cells with Ulex lectin in a three-day-old larva, ventral view. (P) Staining of spinGland and headGland cells with Pisum lectin in a three-day-old larva, ventral view.

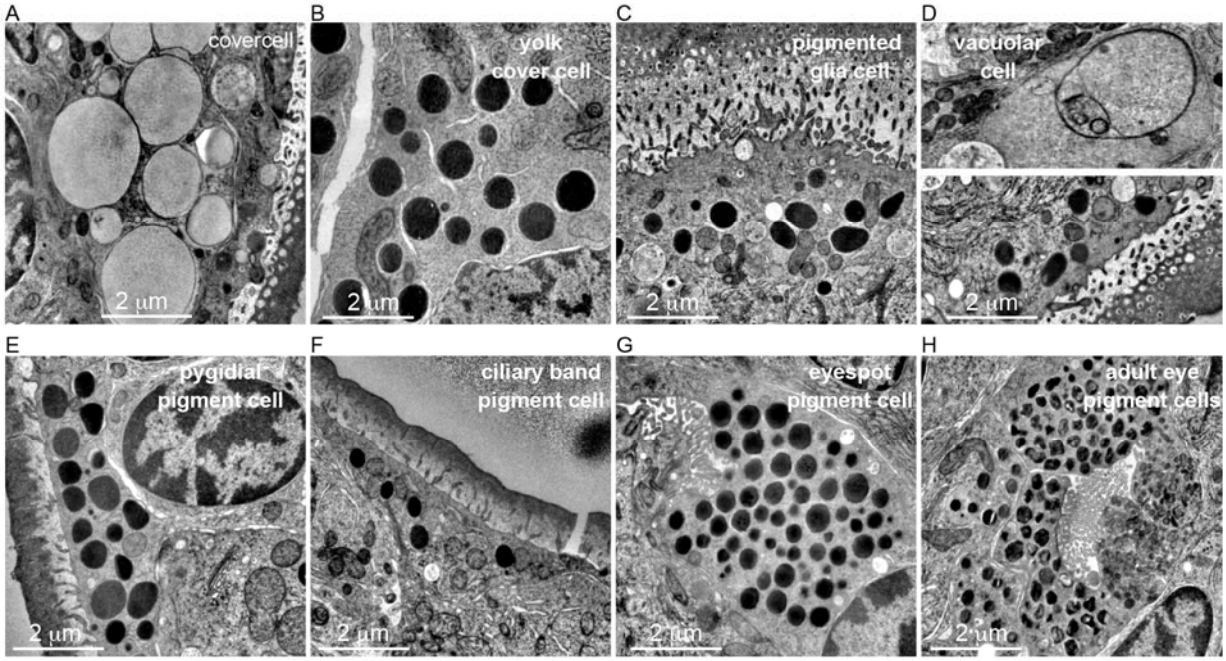

Figure 8 – figure supplement 2. Ultrastructure of pigment cells.

(A) TEM image of a covercell with the large pigment vacuoles. (B) TEM image of a yolk cover cell with large granules. (C) TEM image of a pigmented glia cell. (D) TEM images of a vacuolar cell. (E) TEM image of a pygidial pigment cell. (F) TEM image of a ciliary band pigment cell. (G) TEM image of a pigment cell from the eyespot. (H) TEM image of a pigment cell from the adult eye.

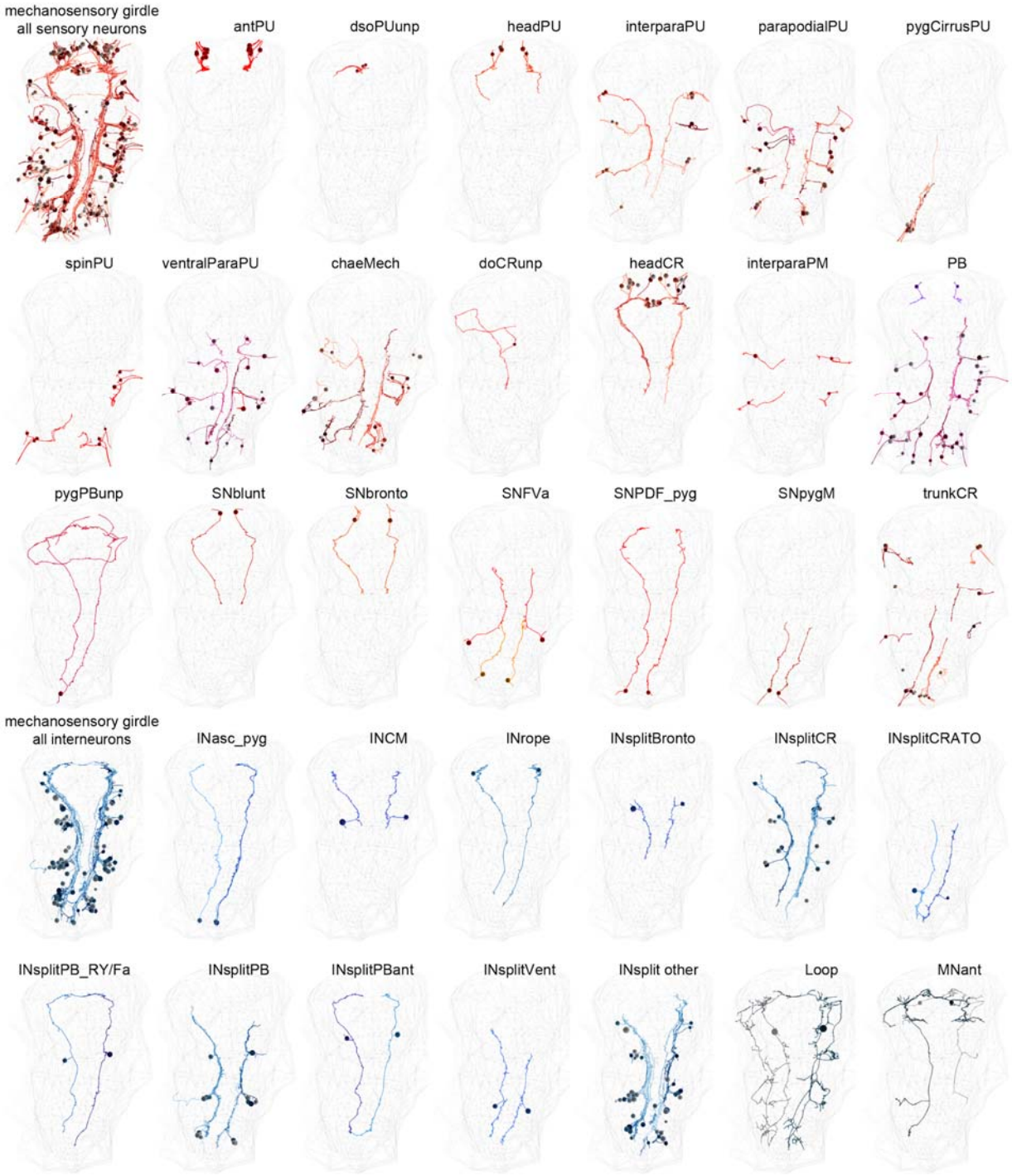

Figure 10 – figure supplement 1. Cell types in the mechanosensory girdle.
EM reconstructions of sensory, inter- and motor neuron types that form the mechanosensory girdle.